U.S. DEPARTMENT OF ENERGY

PNNL-19325

Prepared for the
U.S. Nuclear Regulatory Commission
under an Interagency Agreement
with the U.S. Department of Energy
Under Contract DE-AC05-76RL01830

In-situ Characterization of Cast Austenitic Stainless Steel Microstructure: An Interim Study

P Ramuhalli
LJ Bond
R Mathews
KC Roberts
RV Harris
AA Diaz
M Anderson
CO Ruud

April 2010

Pacific Northwest
NATIONAL LABORATORY

Proudly Operated by Battelle *Since 1965*

DISCLAIMER

PACIFIC NORTHWEST NATIONAL LABORATORY
operated by
BATTELLE
for the
UNITED STATES DEPARTMENT OF ENERGY
under Contract DE-AC05-76RL01830

Printed in the United States of America

Available to DOE and DOE contractors from the
Office of Scientific and Technical Information,
P.O. Box 62, Oak Ridge, TN 37831-0062;
ph: (865) 576-8401
fax: (865) 576-5728
email: reports@adonis.osti.gov

Available to the public from the National Technical Information Service,
U.S. Department of Commerce, 5285 Port Royal Rd., Springfield, VA 22161
ph: (800) 553-6847
fax: (703) 605-6900
email: orders@ntis.fedworld.gov
online ordering: http://www.ntis.gov/ordering.htm


This document was printed on recycled paper.
(9/2003)

PNNL-19325

Ultrasonic Characterization of Cast Austenitic Stainless Steel Microstructure: An Interim Study

P Ramuhalli
LJ Bond
R Mathews
KC Roberts
RV Harris
AA Diaz
MT Anderson
CO Ruud

April 2010

Prepared for the
U.S. Nuclear Regulatory Commission
under an Interagency Agreement
with the U.S. Department of Energy
Under Contract DE-AC05-76RL01830

Pacific Northwest National Laboratory
Richland, Washington 99352

Summary

Cast austenitic stainless steel (CASS) that was commonly used in U.S. nuclear power plants is a coarse-grained, elastically anisotropic material. CASS materials were used in selected designs of nuclear power reactor systems for its resistance to corrosion and durability in service. However, the fabrication processes result in a variety of microstructures that are difficult to inspect ultrasonically. The difficulty in reliable ultrasonic nondestructive evaluation (NDE) of CASS components is largely due to detrimental effects of wave interactions with the coarse-grain microstructures inherent to this class of materials.

To address the inspection needs, new approaches that are robust to these phenomena are being sought. However, to enhance the probability of detecting flaws by overcoming the deleterious effects of the coarse-grained microstructure on the interrogating ultrasonic beam, knowledge of the microstructure and the corresponding acoustic properties of the material may be required. The goal of improving the reliability and effectiveness of ultrasonic inspection of CASS components can therefore potentially be achieved by first characterizing the microstructure of these components. The characterization of CASS microstructures must be done in-situ, to enable dynamic selection and optimization of the ultrasonic inspection technique in the field.

This report documents preliminary experiments that investigate potential in-situ ultrasonic and electromagnetic methods for classification and/or characterization of material microstructures in CASS components, when making measurements from the outside surface of the pipe or component. This work is a continuation of ongoing efforts towards in-situ microstructure characterization for CASS components. The focus of this follow-on study was to evaluate additional ultrasonic measurement methods as well as electromagnetic measurement methods and determine if responses from known microstructures can be differentiated.

On the basis of a comprehensive literature evaluation, two ultrasonic-measurement methods and one electromagnetic-measurement method were selected for further investigation in this phase of the effort. The first ultrasonic measurement technique investigated was normal incidence ultrasonic longitudinal-wave backscatter. The second measurement investigated in this study is focused on the application of ultrasonic diffuse fields. In addition, a multi-frequency eddy current technique was selected for evaluation of its potential for microstructure characterization. Scoping experiments were performed to determine the ability of these measurement methods to discriminate between different microstructures in CASS components. The objective was to determine if a more thorough exploration would be justified in progressing toward development of a real-time in-situ characterization approach for CASS materials, to provide feedback for improving ultrasonic in-service inspection methodologies.

The results of the scoping experiments demonstrated the potential of ultrasonic measurements to classify the material type of CASS for two categories of pure consistent microstructures. Given the simple two-class problem of material being either equiaxed-grain material or a columnar-grain material, both normal incidence longitudinal wave backscatter and diffuse field measurements appear to provide a reliable means to discriminate and correctly classify material type. The backscattering measurements and a threshold algorithm classified all examined material samples correctly and indicated a potentially reliable and robust technique. Attributes computed from the diffuse field measurements, along with a threshold algorithm, classified most of the samples (with one exception) correctly. It is possible that the misclassification is due to changes in the diffuse field from the presence of internal flaws/voids in the

specimen. The experiments provided promising results and demonstrated that there is a good basis to believe that potential exists for further development of these techniques for real-time classification of CASS material.

For the same two-class problem, average magnitude and average phase changes as a function of frequency from multi-frequency eddy current measurements also showed potential for microstructure classification. Relative changes in magnitude and phase at three frequencies correctly classified 13 out of 14 material samples. However, the eddy current method is limited in its applicability due to the effective depth of penetration and very low excitation frequencies may be necessary to inspect and characterize typical thick-section CASS components currently used in nuclear power plants.

It is unlikely that a single microstructural characterization method will be successful in an in-situ application due to the diverse nature of CASS microstructures (layering, banding, etc.) and unknown parameters (such as grain size, wall thickness, etc.). An examination of the results obtained in this study shows that by combining information from multiple measurement methods, higher accuracy in microstructure characterization may be potentially achievable. Therefore, it may be necessary to use multiple measurement methods (both ultrasonic and electromagnetic) to achieve the goal of in-situ microstructure characterization.

In developing this investigation further into potential classification techniques of microstructure using in-situ measurements on CASS, work will focus on refining the ultrasonic and electromagnetic measurement protocols, conducting proof-of-concept experiments for shear wave birefringence, and other techniques that can be used to characterize inhomogeneous and anisotropic material. Continuing work includes:

- Verifying repeatability of the experiments, and confirming the results using additional specimens that are representative of the columnar- and equiaxed-grain structure (as well as mixed-grain and layered/banded-grain structures).
- Enhancing diffuse field measurements through more effective coupling, increasing the accuracy of parameter estimates through the use of accurate models of the ultrasonic diffusion phenomenon, and evaluating diffuse field behavior as a function of separation distance between the transmit and receive transducers, as well as at different frequencies.
- Enhancing acoustic scattering estimates by investigating it as a function of incident and receive angle, shear-wave backscatter measurements, computing scattering coefficient estimates over a broader frequency range through the use of broadband transducers employing swept-frequency excitation, and correlating the backscattered energy to microstructural variation as a function of thickness.
- Conducting shear-wave birefringence measurements to determine the presence of anisotropy in the CASS microstructure.
- Evaluating other ultrasonic and electromagnetic methods used for microstructure and material characterization in other applications, that can be leveraged and applied to the CASS microstructural characterization challenge.
- Evaluating algorithms for assessing microstructural parameters (such as mean grain size and grain orientation variations within the material volume of interest) from one or more measurement types.

Assessing the applicability of these techniques to characterizing cast primary circuit components (safe ends, elbows, or pipes) through inspection from the inner-diameter surface.

Acronyms and Abbreviations

A/D	analog-to-digital
CASS	cast austenitic stainless steel
CCSS	centrifugally cast austenitic stainless steel
EPRI	Electric Power Research Institute
HOS	higher order statistics
NDE	nondestructive examination or evaluation
PISC	Programme for the Inspection of Steel Components
PNNL	Pacific Northwest National Laboratory
SAFT	synthetic aperture focusing technique
SCSS	statically cast austenitic stainless steel
SNR	signal-to-noise ratio
SV	shear wave with vertical polarization

Contents

Figures

Tables

1.0 Introduction

CASS that was commonly used in U.S. nuclear power plants is a coarse-grained elastically anisotropic material. The engineering properties of CASS made it a material of choice for selected designs of nuclear power reactor systems. However, the fabrication processes result in a variety of microstructures that are difficult to inspect ultrasonically (Northcott and Dickin 1944; Northcott and McLean 1945; Cumberland 1963; Jeong 1987). The difficulty in reliable ultrasonic NDE of CASS components is largely due to detrimental effects of wave interactions with the coarse-grain microstructure inherent to this class of materials (Jeong 1987; Kupperman et al. 1987; Diaz et al. 1998; EPRI 2005). The interaction of ultrasonic waves with such material results in phenomena such as sound-speed variations, ultrasonic beam re-direction and partitioning, high attenuation and high background acoustic noise caused by scattering, and phase variations across a wave front. These phenomena make reliable and effective ultrasonic inspections of CASS materials extremely challenging.

To address the inspection needs, new approaches that are robust to these phenomena are being sought. However, to enhance the probability of detecting flaws by overcoming the deleterious effects of the coarse-grained microstructure on the interrogating ultrasonic beam, knowledge of the microstructure and the corresponding acoustic properties of the material may be required. The goal of improving the reliability and effectiveness of ultrasonic inspection of CASS specimens can therefore potentially be achieved by first characterizing the microstructure of the component[(a)] (Jeong 1987; Kupperman et al. 1987; Jeong and Ammirato 1989). Doing so can potentially improve:

- Inspectability of a given component, by characterizing the microstructure of a given component, and then matching an inspection method to the characterized microstructure.
- Optimization of ultrasonic inspection parameters for CASS components. Examples include the ability to modify sensor signal processing algorithms to enhance synthetic aperture focusing technique (SAFT) images (Silverstein and Thomas 1993), optimize SAFT probes to improve the signal-to-noise ratio (SNR) (Nageswaran and Whittle 2008), and optimize ultrasonic phased-array inspection systems (such as delay laws to maintain desired beam characteristics (Chatillon et al. 2000), or array probe design parameters (Kono and Baba 2008). Simulation models to better understand ultrasonic wave propagation in polycrystalline materials (Jenson et al. 2009) can potentially be used in the optimization process (Connolly et al. 2008a).
- Interpretation of measured ultrasonic data through the application of appropriate signal processing tools to improve the SNR, thereby enhancing flaw detection and discrimination.
- Probabilistic Risk Assessment (PRA), both directly through knowing the microstructure, and indirectly through improved inspection reliability.

The characterization of CASS microstructure must be done in-situ, to enable dynamic selection and optimization of the ultrasonic inspection technique.

([a]) Hildebrand BP, MS Good, and AA Diaz. 1991. *Ultrasonic Classification of Centrifugally Cast Stainless Steel Utilizing the Rayleigh Critical Angle Technique*. Technical Letter Report from PNNL to the NRC.

1.1 Objectives of this Report

This report documents scoping experiments that investigate potential in-situ ultrasonic and electromagnetic methods for classification and/or characterization of material microstructures in CASS components, when making measurements from the outside surface of the pipe or component. This report is a continuation of earlier efforts towards in-situ microstructure characterization that are documented in Ramuhalli et al. (2009). This earlier study focused on the use of ultrasonic longitudinal-wave attenuation, and the time-of-flight ratio between normal incidence shear waves and normal incidence longitudinal waves for discriminating between two distinct microstructure classes. The focus of the present study was to evaluate additional ultrasonic measurement methods as well as electromagnetic-measurement methods and determine if responses from known microstructures can be differentiated.

A comprehensive literature survey, documented by Ramuhalli et al.,[(a)] was conducted to determine the range of interactions between coarse-grained material on ultrasonic waves and their impact on nondestructive evaluation. On the basis of this literature evaluation, two ultrasonic measurement methods were selected for further investigation in this phase. The first ultrasonic measurement investigated in this follow-on study was normal incidence ultrasonic longitudinal-wave backscatter. The second portion of this study focused on the use of ultrasonic diffuse fields.

A survey of CASS fabrication methods (Ruud et al. 2009) also revealed a potential variation in delta ferrite composition between the different microstructures common to CASS. Because delta ferrite impacts the magnetic permeability of CASS components, nondestructive methods that are sensitive to magnetic permeability variations are also potential candidates for microstructure characterization (ASNT 2004). The most common of these methods (and one currently used in operational nuclear power plants for in-service inspection) is the multi-frequency eddy current technique, and it was selected for further evaluation of its potential for microstructure characterization.

Scoping experiments were performed to determine the ability of these measurement methods to discriminate between different microstructures in CASS components. The objective was to determine if a more thorough exploration would be justified in progressing toward the development of a real-time in-situ characterization approach for CASS materials, and to use this feedback to further improve ultrasonic in-service inspection methodologies. The results of this preliminary study are presented in this report.

1.2 Organization of the Report

The rest of this report is organized as follows.

- Section 2 provides a brief discussion of CASS materials, and summarizes the background for the ultrasonic and electromagnetic methods evaluated in this study.
- Section 3 describes experiments to evaluate two qualitative ultrasonic measurements as a means of discriminating between two very different CASS microstructures – equiaxed-grain microstructures and columnar-grain microstructures. The ultrasonic measurements selected for this study were normal incidence longitudinal wave backscatter, and diffuse field measurements. Details of the

([a]) Ramuhalli P, RV Harris, Jr., LJ Bond, MS Good, AA Diaz, CO Ruud, and MT Anderson. 2010 (to be published). *Ultrasonic Characterization of CASS: Review and Prospects*. Prepared for the U.S. Nuclear Regulatory Commission by Pacific Northwest National Laboratory, Richland, Washington.

specimens, experiments, and data analysis, along with a discussion of the results, are provided in this section.

- Section 4 describes experiments to evaluate multi-frequency eddy current measurements as a means of discriminating between purely equiaxed-grain material and purely columnar-grain material. Details of the specimens, experiments, and data analysis, along with a discussion of the results, are provided in this section.
- Section 5 summarizes the results and provides recommendations for further investigation.
- Section 6 contains references cited in this document.

2.0 Cast Austenitic Stainless Steel

CASS commonly used in nuclear power plants is a polycrystalline coarse-grained material that is elastically anisotropic. The interaction of ultrasonic waves with such material results in phenomena such as sound speed variations, ultrasonic beam redirection and partitioning, large direction-dependent attenuation and background acoustic noise caused by grain-induced scattering, and phase variations across a wave front. These phenomena make reliable ultrasonic inspections extremely challenging but can potentially form the basis for methods of classifying and characterizing CASS microstructures based on the acquisition and analysis of ultrasonic signatures (measurements).

Variations in composition and fabrication processes can also result in electric conductivity and magnetic permeability variation across CASS microstructures. The variation in electromagnetic properties of CASS components can potentially form the basis for the use of electromagnetic signatures (measurements) for classifying and characterizing CASS microstructures.

This section provides a brief review of CASS material microstructures, followed by a discussion of potential ultrasonic and electromagnetic measurements for in-situ microstructure classification and characterization.

2.1 CASS Material

CASS components, unlike wrought austenitic stainless steel, are typically cast to a near net shape of the final component dimensions. Statically CASS (SCSS) components are typically large and the sand-cast mold insulates the solidified metal. A coarse-grain material results from the slower cooling rate and the microstructure not being refined. A rotating casting mold is used during centrifugally CASS (CCSS) piping fabrication. Microstructure and macrostructure are affected by material chemistry, mold and metal temperatures, metal pour rate, cast rotation rate, and mold vibration (Northcott and Dickin 1944; Northcott and McLean 1945; Cumberland 1963). Macrostructure includes the homogeneity of the microstructure, texture for direction-dependent features, and residual stresses (Goebbels 1994). Similar comments may be made for other austenitic stainless steel portions of the reactor system that employ cast-like fabrication methods. This includes regions such as welds, weld overlay repair of welds, and differential welds where a weld bead is applied and dendrites form during solidification.

The following characteristics may be observed in various specimens (Ruud et al. 2009):

- Variable grain sizes and shapes, depending on casting methods and parameters
  - Uniform radially oriented columnar grains
  - Uniformly equiaxed with no directional preference
  - Eclectic mixture of columnar and equiaxed grains
  - Variation radially by layer (banding), with bands possible
  - Variation by axial and circumferential position within a given component
- Unpredictability of exact microstructure, even knowing the casting methods used
- Significant delta ferrite content.

2.2 Ultrasonic Wave Behavior in CASS

In general, in coarse-grained materials, acoustic wave propagation is a function of the microstructure, frequency, and wave mode[(a)] (Auld 1973; Kupperman et al. 1981; Jeong 1987; Kupperman et al. 1987; Thompson et al. 2008; Ensminger and Bond 2010). Coarse-grained materials can have random equiaxed, columnar, or mixed grain structures. Depending on the frequency (or, equivalently, wavelength) and mode of the acoustic wave, a range of behaviors may be observed in all of these grain structures. For instance, equiaxed grain structures will typically result in attenuation, scattering, and beam distortion. In an equiaxed material, this behavior will be largely independent of the angle of incidence. On the other hand, in columnar (transversely isotropic) grains, the result is dependent on the incidence angle relative to preferred grain orientation. Waves propagating along the preferred orientation direction will be minimally attenuated. Beam redirection and partitioning may take place depending on the mode used and the direction of initial propagation. Transverse to the columns, the material behaves as an equiaxed material. Lower frequencies, where wavelengths are large compared to the mean grain size, tend to have the lowest attenuation because the material-ultrasonic wave interaction is in the quasi-Rayleigh regime.

Anisotropy in materials such as CASS can arise from texture/structure (grain size and orientation), composition variations and contamination, stress, or deformation. Texture anisotropy appears to have the highest impact on ultrasonic wave propagation, followed by stress (Segura et al. 2009). The anisotropic nature of CASS materials can significantly impact ultrasonic wave propagation in the material, depending on the choice of the wave mode used. Longitudinal (L) wave probes are commonly used due to issues of ray skew, backscatter, and attenuation inherent to vertically polarized shear (SV) waves when used in coarse-grain material or strongly textured material. However, the use of shear waves, while relatively uncommon in these materials, may provide additional information for microstructural characterization.

Several authors have investigated the various phenomena inherent in acoustic wave interaction with anisotropic coarse-grained materials such as CASS. Theoretical studies based on the use of both semi-analytical models and simulation models have been performed by several authors with a view to better understanding the behavior of ultrasonic wave propagation in coarse-grained materials such as CASS (for instance, Ogilvy 1988; Harker et al. 1990; Chassignole et al. 2008; Connolly et al. 2008a, b; Doudet et al. 2008; Thompson et al. 2008; Chassignole et al. 2009; Connolly et al. 2009). Phenomena that have been documented include beam deviation or skew (for instance, Auld 1973; Kupperman et al. 1981; Jeong 1987; Kupperman et al. 1987; Figures 5 and 7 from Connolly et al. 2009), phase distortion of the acoustic wave front (for instance, Bordier et al. 1991; Good et al. 1991; Thompson et al. 2008), and attenuation (for instance, Kupperman et al. 1981; Ramuhalli et al. 2009). A detailed discussion of acoustic wave behavior in coarse-grained anisotropic materials, particularly CASS, along with a comprehensive bibliographical listing of relevant literature, is presented in Ramuhalli et al.[(a)]

The phenomena discussed above have a deleterious effect on the ultrasonic signal from CASS specimens. However, they can form the basis for measurements that can classify the microstructure of CASS components. In this study, ultrasonic backscatter and diffuse field measurements are investigated further.

([a]) Ramuhalli P, RV Harris, Jr., LJ Bond, MS Good, AA Diaz, CO Ruud, and MT Anderson. 2010 (to be published). *Ultrasonic Characterization of CASS: Review and Prospects*. Prepared for the U.S. Nuclear Regulatory Commission by Pacific Northwest National Laboratory, Richland, Washington.

2.2.1 Ultrasonic Backscatter

Acoustic wave interactions with materials depend on mechanical properties of the material (Pao 1983) such as density and elastic constants. Variability in the spatial distribution of these properties results in an inhomogeneous material, with resulting spatial variability of the acoustic properties (velocity, acoustic impedance, etc.). In contrast, directional variability results in an anisotropic material, the acoustic property being a function of direction of propagation. Fine-grained materials are often quasi-isotropic and quasi-homogeneous, because the granular anisotropies and inhomogeneities are at a scale that is relatively small compared to the wavelengths of interest and crystallographic axes of grains are randomly oriented. In coarse-grained materials, the large grain sizes result in significant local inhomogeneity, and preferred orientation of the grains, coupled with inherent anisotropies in each grain, can result in significant anisotropy.

As acoustic waves interact with materials, scattering of energy occurs at interfaces such as grain boundaries. Scattering in the direction of the transmitting transducer is often referred to as backscatter. However, the scattered energy at any angle (relative to the transmit direction) can be measured, if a receiver can be placed appropriately. Scattering typically occurs if the mean scatterer (grain) size ($\bar{D}$) is small or comparable to the wavelength λ of the acoustic wave, and a change in acoustic impedance is present across the grain boundary (Goebbels 1994). The contrast in acoustic impedance across a grain boundary can occur due to anisotropy of the elastic properties of grains and the different orientation of each grain (Thompson et al. 2008). In general, the scattering behavior of ultrasonic waves from single scatterers may be broadly classed into three regimes (Ensminger and Bond 2010) – Rayleigh, stochastic, and geometric. In the Rayleigh regime, the scatterer or grain size (d) is small relative to the wavelength of the acoustic wave used [typically, $d/\lambda \ll 1$ (Goebbels 1994)]. As the ratio of the grain size-to-wavelength increases, the interactions between the wave and the grains increases, resulting in increased amounts of scattering. In the large-grain limit ($d/\lambda \gg 1$), where the wavelength is much smaller than the grain size, the scattering behavior may be described using geometric principles. For intermediate wavelengths, however, the observed acoustic behavior is best described using stochastic methods. In CASS materials, the grain sizes can vary over a large range[(a)] and, therefore, the scattering behavior can range from Rayleigh to geometric regimes in a single material volume. Thus, the mean grain size $\bar{D}$ is often used instead of the individual grain size d to describe the scatterer size and the dominant scattering regime.

Backscatter measurements have been used for a range of material characterization applications. The backscattered signal has been correlated with grain size (Willems and Goebbels 1982; Feuilly et al. 2009), though the technique is not recommended for large grains and significant acoustic path where multiple scattering is significant. Moysan and Corneloup (2000) discuss the use of backscatter attenuation to characterize texture and orientation in transversely isotropic welds. Backscattered acoustic signals from annealed polycrystalline aluminum possess fractal characteristics (Barat et al. 1998), and a grain-size distribution can be deduced to match the distribution obtained experimentally in polycrystalline materials. Miralles et al. (2004) and Miralles and Vergara (1999) present a different approach to grain structure/size determination using backscatter. They use higher order statistics (HOS) and derive relations between the

(a) Diaz AA, AD Cinson, SL Crawford, RA Mathews, TL Moran and MT Anderson. 2010. *An Evaluation of Ultrasonic Phased Array Testing for Cast Austenitic Stainless Steel Pressurizer Surge Line Piping Welds*. Draft NUREG/CR and PNNL report. Prepared by Pacific Northwest National Laboratory for the U.S. Nuclear Regulatory Commission.

material and transducer parameters, and the first, second, and third order cumulants of the backscattered signal.

The ability to time-gate a signal and select backscatter from a specific region in the material may make backscattering attractive for CASS microstructure characterization. However, it is not clear if such an approach will work for materials with strong multiple scattering, and in such cases, the backscattered measurement may only be indicative of bulk properties. Note that, with multiple scattering, the backscatter measurement shows a peak that is delayed relative to the single scattering case (Turner and Weaver 1995), and the delay is a function of the grain size, angle of incidence and measurement, and the frequency. It is also not clear how scattering measurements may apply to coarse-grained materials, where there may be only a few grains that the ultrasonic beam interacts with prior to reflection from the back surface (Goebbels 1980). In such a case, it is possible that the scattered field will resemble the single-scattering scenario more than the strong multiple-scattering scenario. In CASS materials (or in anisotropic inhomogeneous materials in general), the beam redirection and partitioning that is likely to occur, particularly with angle-beam incidence, makes microstructure characterization using angle-beam incidence a difficult proposition, if the goal is to classify microstructure as a function of depth/location.

Given these constraints, the choice of wave mode and frequency (or, equivalently, wavelength) for scattering measurements becomes critical. Assuming that an appropriate frequency can be identified, the hypothesis is that polycrystalline equiaxed microstructures should generally be correlated with higher backscattered energy due to the coarse-grained nature of the microstructure, the random orientation of grains, and the typically rather large ratio of grain size-to-wavelength. At higher frequencies (geometric to stochastic scattering regimes), this will likely result in multiple scattering and a correspondingly higher backscatter signal. For columnar grains with incidence along the grain axis, the combination of a lower attenuation and preferential wave propagation direction should, theoretically, result in a lower overall backscatter measurement. Note that the above discussion is valid only for normal incidence (and in columnar grains, incidence along the axis of the grains).

2.2.2 Diffuse Fields

Diffuse field measurements are related to the scattering phenomena discussed above. When a material is insonified with ultrasonic energy, acoustic impedance mismatches at the grain boundaries results in a portion of the energy being scattered before returning to the receiving transducer. At times that are large when compared to the first direct reflection (Weaver and Lobkis 2001), the propagation behavior of the scattered energy satisfies a diffusion equation and the resulting field measurement is referred to as the diffuse field measurement. However, the diffuse field measurement is a stochastic quantity due to the random nature of the multiple scattering (Weaver and Lobkis 2000).

Theoretical analysis and modeling of the diffuse field phenomenon has been done by several researchers (Weaver 1982; Turner and Weaver 1995; Turner 1999; Sgard et al. 2000; Weaver and Lobkis 2001, 2004, 2005; Ghoshal and Turner 2009). The diffuse field depends on a range of factors including temperature (Weaver and Lobkis 2000). Ramamoorthy et al. (2004) provide an analytical (parametric) solution to the 2-D diffusion equation in a slab with rectangular cross-section as:

$$E(x,y,t)=\left\{1+\sum_{n=1}^{\infty}\sum_{m=1}^{\infty}4\cos\left(\frac{n\pi x_0}{l}\right)\cos\left(\frac{n\pi y_0}{p}\right)\cos\left(\frac{n\pi x}{l}\right)\cos\left(\frac{n\pi y}{p}\right)e^{-D\left[\left(n\pi/l\right)^2+\left(m\pi/p\right)^2\right]t}\right.$$
$$+\sum_{m=1}^{\infty}2\cos\left(\frac{n\pi x_0}{l}\right)\cos\left(\frac{n\pi x}{l}\right)e^{-D\left[\left(n\pi/l\right)^2\right]t} \qquad (2.1)$$
$$\left.+\sum_{m=1}^{\infty}2\cos\left(\frac{n\pi y_0}{p}\right)\cos\left(\frac{n\pi y}{p}\right)e^{-D\left[\left(m\pi/p\right)^2\right]t}\right\}E_0e^{-\sigma t}$$

Here, l and p are the length and thickness of the specimen (the width is assumed to be very large in comparison to the length and thickness, enabling the application of a 2D approximation). The transmitting transducer position is given by (x_0, y_0), the receiving transducer is placed at (x,y), E_0 is the initial energy deposited at time t = 0, D is the ultrasonic diffusivity measured in units of length squared per time, and σ is the dissipation (measured in units of inverse time). $E(x,y,t)$ is the ultrasonic spectral energy density. This equation may be used, along with the measurements, to estimate the diffusivity and dissipation if the other quantities are known.

Diffuse field measurements have been proposed for a range of characterization applications, from rocks (Scales and Malcolm 2003; Malcolm et al. 2004) to polycrystalline metals (Weaver 1982; Turner 1999; Ghoshal and Turner 2009). Diffuse field measurements have been applied in the experimental characterization of high scattering materials with random structure such as cement-based materials (Becker et al. 2003) and have been shown to correlate with crack length in concrete (Ramamoorthy et al. 2004). Diffuse fields have also been studied in polycrystalline media (Turner and Weaver 1995). These studies present both theoretical development of diffuse field theory and some experimental verification of the diffuse field phenomenon. Multiple scattering is typically considered in any diffuse field theoretical development. Ghoshal and Turner (2009) discuss the theoretical investigation of backscatter in polycrystalline materials. Similar measurements for semi-solid materials (such as slurries) have also been conducted, with diffusion parameters recovered from the data (Weaver and Sachse 1994). In all cases, the key parameters that are computed from the diffuse field data are the diffusivity and dissipation. These quantities depend on factors such as the grain size and the frequency, which also influence the peak arrival time of the diffuse field energy at the receiving transducer. While these (and other similar) studies have shown the diffuse field phenomenon in highly scattering anisotropic materials, there appears to be little effort in the characterization of material microstructure from diffuse field data.

CASS materials, as discussed earlier, are elastically anisotropic and heterogeneous. The coarse-grained nature of CASS, along with its anisotropic nature, results in higher scattering analogous to that in materials such as cement, rock, and other polycrystalline materials. It is however, not clear how the presence of columnar grain structures impacts the diffuse field measurement. It is likely that in equiaxed materials, diffusivity will be high due to the random orientation of the microstructure, resulting in higher scattering in all directions. This should, in turn, correspond to a faster arrival time at the receiving transducer. Columnar grains will likely result in preferential directions for wave propagation, resulting in lower diffusivity corresponding to longer arrival times.

2.3 Electromagnetic Interactions in CASS

Consider an eddy current measurement system, as shown in Figure 2.1. A coil, excited with an alternating current at a specific frequency, is used to induce eddy currents in accordance with Lenz's law (ASNT 2004), in the specimen under test. The corresponding induced magnetic flux density changes the net flux linked with the coil, resulting in a change in its inductance. At the same time, losses due to the induced currents in the specimen manifest themselves as an increase in the resistance of the coil. Thus, an eddy current coil will present a change in electric impedance (relative to its impedance in air) when placed near a conducting specimen.

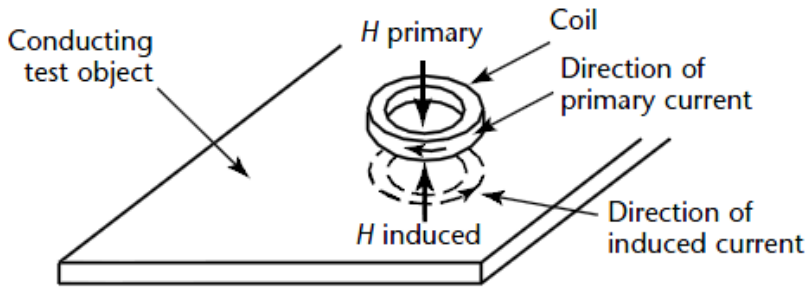

Figure 2.1. Schematic of Eddy Current Inspection of CASS Specimens (ASNT 2004). © 2004, the American Society for Nondestructive Testing, Inc. Reprinted with permission from the *Nondestructive Testing Handbook*, Third Edition: Vol. 5, *Electromagnetic Testing*.

Differences arise between the eddy current measurements over ferromagnetic and non-ferromagnetic specimens. In the case of non-ferromagnetic specimens, the presence of the specimen (and therefore the induced currents) results in a decrease in the inductance with an increase in the resistance. However, for ferromagnetic specimens, the inductance typically increases as well (ASNT 2004) with an increase in magnetic permeability. This forms the basis for most permeability measurement systems as well as for instruments that measure ferrite levels using the magnetic permeability variations.

Three other factors (besides the permeability) also play a role in determining the response of eddy current measurements in ferromagnetic specimens. These are the conductivity, probe liftoff, and frequency. Figure 2.2(a) shows the direction of change in the impedance due to increasing liftoff. For ferromagnetic specimens, this is seen to be in the direction opposite that of increasing permeability. Increasing conductivity also generally results in a change in the response [Figure 2.2(b)]. Finally, for a constant permeability, liftoff, and conductivity, the effect of changing frequency is to rotate the signal [Figure 2.2(c)].

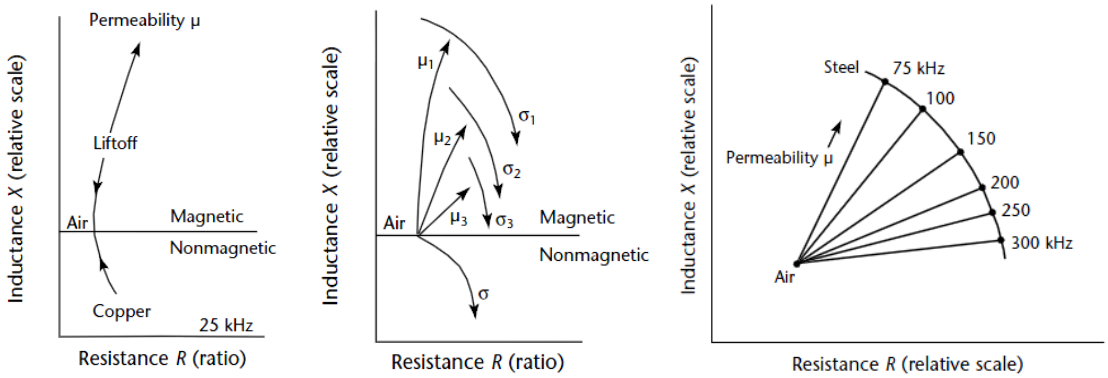

Figure 2.2. Impedance Trajectories as a Function of Permeability and (a) Liftoff, (b) Conductivity, and (c) Frequency. In part (b), subscript 1 refers to ferrites, subscript 2 refers to steel, and subscript 3 refers to nickel (ASNT 2004). © 1983, 2004, the American Society for Nondestructive Testing, Inc. Reprinted with permission from the *Nondestructive Testing Handbook*, Third Edition: Vol. 5, *Electromagnetic Testing*.

As the eddy current excitation frequency increases, the skin depth (or standard depth of penetration of the eddy currents) decreases (ASNT 2004). The standard depth of penetration is defined as

$$\delta = \sqrt{\frac{1}{\pi f \mu \sigma}} \tag{2.2}$$

where f is the excitation frequency, μ is the permeability of the material and σ is the conductivity. For non-ferritic steel, the skin depth at 1 kHz is about 13.1 mm (0.52 in.). In CASS materials, the ferrite content varies both with microstructure as well as over the surface and through the thickness of the specimen. Thus, the permeability will also vary according to microstructure and casting processes, and with location within the specimen, and in general, is not known a priori. Thus, quantifying the exact skin depth in CASS components is difficult.

As discussed earlier, the casting process for CASS materials results in a range of microstructures, with differing levels of ferrite content. Based on other studies (Temple and Ogilvy 1992), the hypothesis is that equiaxed microstructures will, in general, have higher ferrite content and a correspondingly higher magnetic permeability. The result should be a higher eddy current magnitude for equiaxed specimens. In addition, changes in composition (and permeability) may result in differences in the phase of the eddy current measurement between equiaxed and columnar microstructures.

3.0 An Evaluation of Potential Ultrasonic In-Situ Characterization Methods

The discussion in the previous section highlights the possibility of using ultrasonic measurements from the outer surface for in-situ characterization of CASS microstructures, and ultrasonic experiments were designed to test this hypothesis. A two-class discriminant problem was postulated where CASS macrostructure was either equiaxed-grain or columnar-grain material. If data and analysis provided a means to successfully sort material into these two classifications, then justification to develop a more thorough and staged exploration would exist. The two ultrasonic measurements proposed for the experiment were normal incidence longitudinal-wave backscatter and diffuse field measurements. Details of these measurements are provided in this section.

3.1 Centrifugally CASS Specimens

Five specimens (Figure 3.1) were selected from an assortment of PNNL samples that had been previously used in PNNL studies (Heasler and Doctor 1996) as well as for Action 4 of the Programme for the Inspection of Steel Components III (PISC III) (Bates et al. 1987). The PISC III specimens consisted of a welded pipe section with a girth circumferential weld joining two pipe sections of equiaxed-grain and columnar-grain material, respectively (Figure 3.1 and Figure 3.2). A stamped label (B510, B516, B517, B518, and B527) uniquely identified each specimen. These five specimens (consisting of a total of five material volumes of equiaxed-grain material and five volumes of columnar-grain material) were used to obtain ultrasonic measurements, with the measurement locations selected to avoid edge effects and any surface anomalies. Typical axial, radial, and circumferential arc length dimensions of a specimen were 40 cm (15.75 in.), 5.9 cm (2.32 in.), and 18 cm (7.09 in.), respectively. Pipe wall thickness of the columnar material typically ranged between 59.9 mm and 60.5 mm (2.36–2.38 in.) while that of the equiaxed material typically ranged between 57.7 mm and 57.9 mm (2.27–2.28 in.).

Figure 3.1. Selected PISC III Specimens Used for Ultrasonic Measurements. Each specimen is a welded assembly of two pipe sections where one material was an equiaxed material and on the opposite side of the weld was a columnar material.

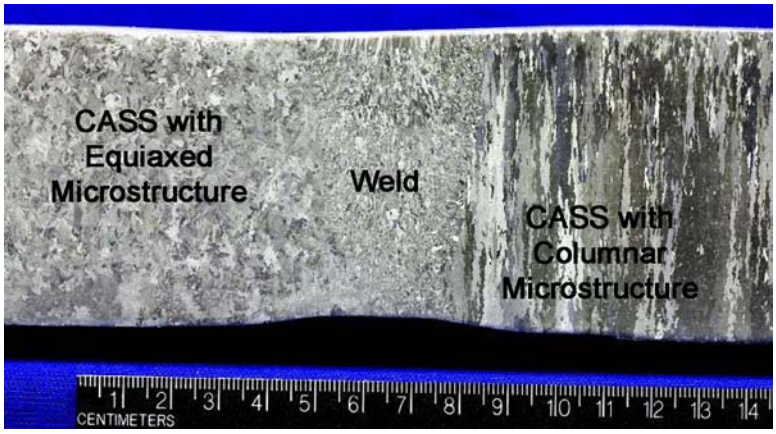

Figure 3.2. A Representative Axial-Radial Cross Section of a CCSS Specimen from the PISC III Studies, Showing Typical Outside and Inside Diameter Geometry, and Microstructure of a Specimen. The equiaxed CCSS grains on the left have a mean lineal intercept of 2.34 mm (0.092 in.) and the columnar CCSS grains on the right have a mean lineal intercept of 2.48 mm (0.097 in.). The mean lineal intercept is the average length of a line segment that crosses a sufficiently large number of grains. It is proportional to the equivalent diameter of a spherical grain (Steele and McCall 1984).

3.2 Ultrasonic Backscatter

3.2.1 Backscatter Experimental Setup

The first parameter measured was normal incidence longitudinal-wave backscatter. The experimental setup used a RITEC (RITEC, Inc., Warwick, Rhode Island) square-wave pulser (model SP-801), broadband receiver (model BR-640), diplexer (RDX-2), and a focused immersion ultrasonic transducer operating at 2.25 MHz (Panametrics V395, 38.1-mm (1.5-in.) diameter, 230-mm (9.06-in.) focal length. The ultrasonic transducer was employed to generate normal incidence longitudinal waves. The transducer was operated in pulse-echo mode. A simulation using Imagine3D[(a)] (Version 2.5) was conducted to identify the defocus distance that would ensure that the ultrasonic energy was focused on the back-surface (Figure 3.3). The simulation indicated that the optimal defocus length was approximately −127 mm (−5 in.) (the negative sign indicates that the transducer was moved towards the specimen). This information was used to determine placement of the transducer above the outer surface of the specimen. A mechanical scanner was used to record the backscatter signal over a 12.7-mm × 12.7-mm (0.5-in. × 0.5-in.) region, with a step size of 2.54 mm (0.1 in.). Data was acquired using an 8-bit computer-controlled analog-to-digital (A/D) converter (Gage Compuscope CS82g), using a sampling rate of 100 MHz. The experimental setup is shown in Figure 3.4. At every position, eight waveforms were averaged to improve the SNR. The recorded A-scan contained the specular front-surface reflection and was of sufficient length to ensure that the acoustic path length was at least four times the specimen thickness (corresponding to at least two back-surface reflections). The instrument settings (receiver gain of 52 dB, receiver bandwidth of 2 MHz, corresponding to the frequency range from 1 MHz to 3 MHz) were held constant regardless of the specimen and microstructure being investigated. This enabled a direct comparison of the measurements from the different specimens.

[a] http://www.utex.com

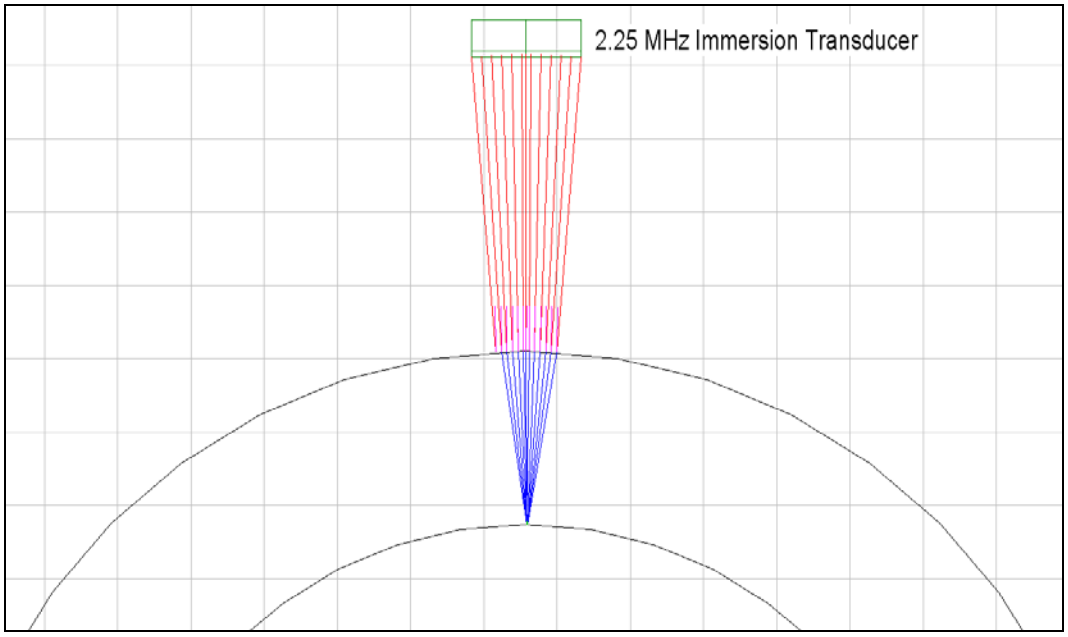

Figure 3.3. Simulation (using Imagine3D) of Energy Propagation from a Spherically Focused Immersion Ultrasonic Transducer (230-mm or 9.06-in. focal length) into a 60-mm (2.36-in.)-Thick Pipe Section. The transducer is defocused (moved towards the specimen) by 127 mm (5 in.), resulting in energy focusing on the back surface. The grid size in the figure is 25.4 mm (1 in.).

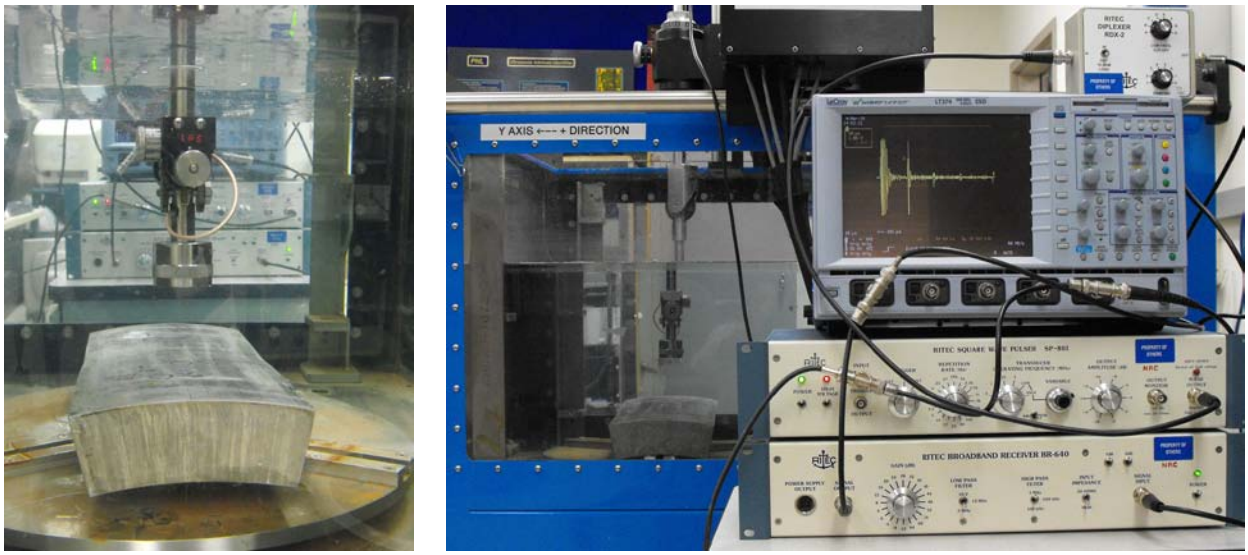

(a) (b)

Figure 3.4. Experimental Setup for Backscatter Measurement. (a) Specimen and transducer in immersion tank; (b) ultrasonic pulser and receiver, with the A-scan displayed on an oscilloscope. The data acquisition was performed using a computer-controlled A/D converter card and related data acquisition software.

3.2.2 Backscatter Data Analysis

Figure 3.5 presents examples of the backscattered ultrasonic A-scans (at 2.25 MHz) measured from the center of the scan region, for equiaxed and columnar regions. The time gate chosen in Figure 3.5(a) displays the entire A-scan from the front-surface reflection, and the horizontal axis has been scaled to show distance (assuming a nominal sound speed in CASS materials of 5800 m/s [2.28×10^5 in./s]). The two A-scans shown in the figure have been aligned in time, and the difference in the arrival time of the back-wall reflection highlights the different specimen thicknesses as well as potential differences in longitudinal wave speed in equiaxed and columnar microstructures. Figure 3.5(b) shows the signal between the front-surface and the first back-surface reflection and clearly shows the higher backscattered energy in equiaxed materials.

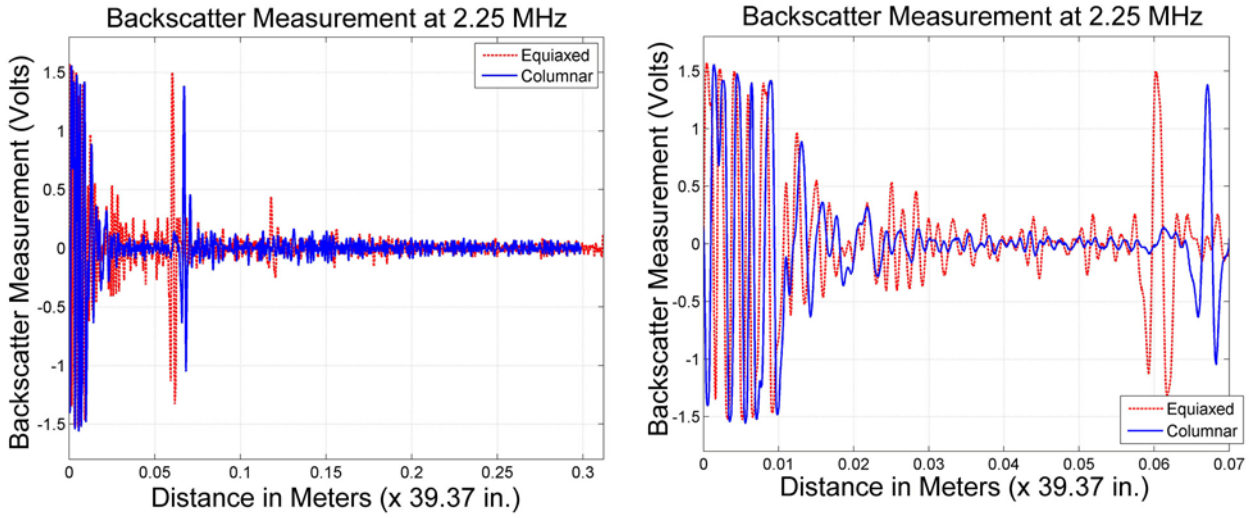

Figure 3.5. Examples of A-scans from Columnar and Equiaxed Regions. (a) Recorded A-scan; (b) expanded view showing backscattered energy during the first pass through the specimen. The data were recorded on specimen B510.

The data in the figure show significant variation in the backscattered amplitude of the A-scans as a function of time (or, equivalently, distance). This variation is likely due to the fact that each microstructure sees a different mean field and scatters differently based on the grain size, shape, orientation, and spatial distribution. The use of spatial averaging (Goebbels 1986, 1994), which is based on an ergodic hypothesis (i.e., the ensemble average is the same as a spatial average), can account for this variation when computing the backscattered energy. Parameters such as the attenuation and backscatter coefficient can then be computed from the backscattered energy, and correlated with quantities such as grain size (Goebbels 1980, 1986, 1994). The spatial averaging approach was investigated in this study. Details of the processing algorithm are presented here.

1. For each position of the transducer, the backscattered energy was computed by first squaring the A-scan data, and then low-pass filtering the result. Squaring the signal shifts the frequency content of the measurement towards the baseband, and also replicates it at a higher frequency (twice the center frequency of the transducer or 4.5 MHz). A low-pass filter is therefore an

effective means of extracting the energy (the envelope) of the signal. While smaller cutoff frequencies (on the order of several kHz) can be used to extract the envelope, the use of spatial averaging in this instance also achieves a similar goal. Therefore, for the data in this study, a cut-off frequency of 2.25 MHz was used.

2. The computed backscatter energy signals from a region around the transducer position were averaged. While the size of this neighborhood region can vary depending on the application, in this study, the neighborhood size was selected to be 12.7 mm × 12.7 mm (0.5 in. × 0.5 in.), corresponding to the entire scan size.
3. The resulting backscattered energy response between the front surface and back-surface reflections was used as the input to a least-squares curve fitting algorithm. The assumed form of the backscatter energy was

$$y = Ae^{-\alpha x}, \tag{3.1}$$

where y is the backscattered energy, x is the distance, A is an unknown quantity proportional to the scattering coefficient, and α is the (unknown) attenuation coefficient. This expression assumes a single scattering scenario (Goebbels 1980) in an isotropic homogeneous medium. The data selected to estimate the parameters corresponded to the backscatter measurement between the front-surface reflection and the first back-surface reflection, to avoid fitting a curve using saturated measurements.

The measurements in this study were taken with the transducer focused approximately on the back-surface and no diffraction correction was applied. The need for diffraction correction of the backscattering measurements from this experimental setup needs to be studied further.

3.2.3 Backscatter Results

Figure 3.6 shows the backscattered energy at 2.25 MHz using the averaging procedure described in the previous section. The data clearly show a separation between measurements from the two distinct microstructures. The differences are clearer when using a logarithmic scale (Figure 3.7). The backscatter energy from equiaxed microstructures is seen to be much higher than that from columnar regions. Figure 3.8 shows the results of the exponential curve fitting. In this figure, the data (between the front- and back-surface reflections) are shown along with the fitted curve (the data are presented on a logarithmic scale to enhance the differences between the measurements). Backscattered energy from columnar regions is seen to decay faster while backscattered energy from equiaxed regions decays slower. In both cases, the backscattered energy deviates from a pure exponential decay (after about 2 cm [0.79 in.] into the material). This behavior is indicative of multiple scattering (Goebbels 1980; Thompson et al. 2008).

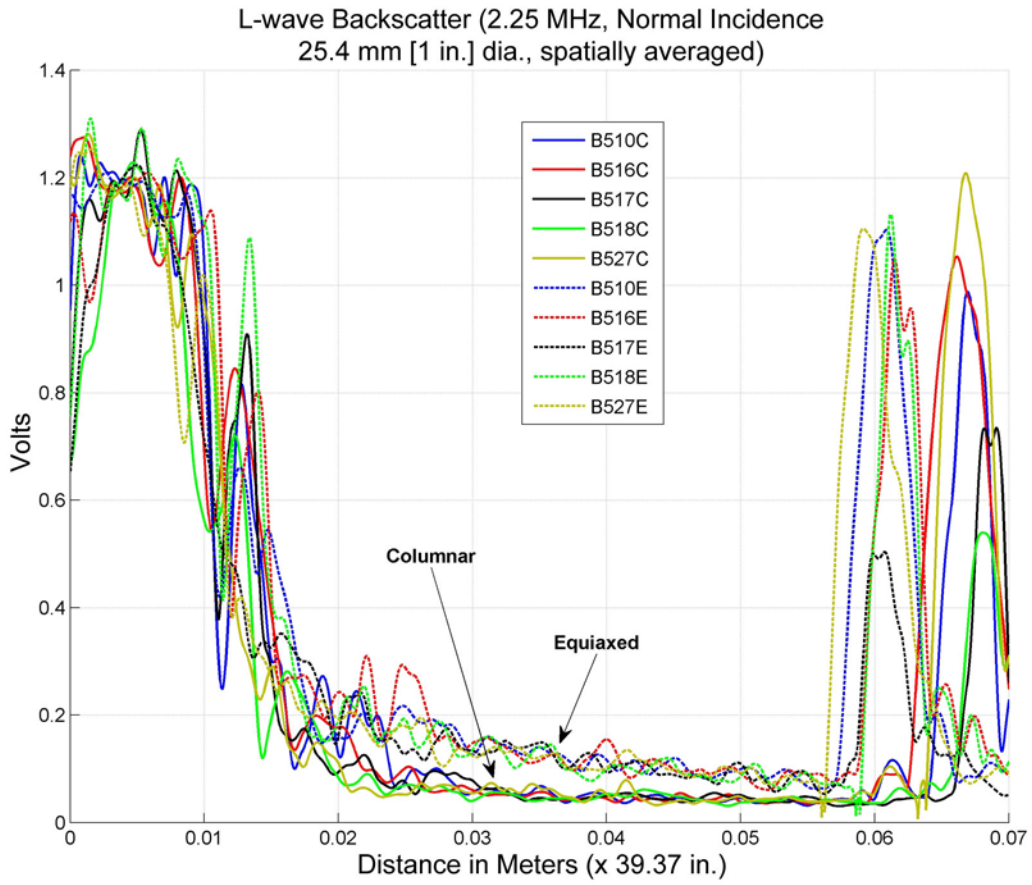

Figure 3.6. Backscatter Energy as a Function of Distance (acoustic path length) Assuming a Nominal Wave Speed of 5800 m/s (2.28×10^5 in./s). Differences between backscattered energy from equiaxed and columnar regions are apparent.

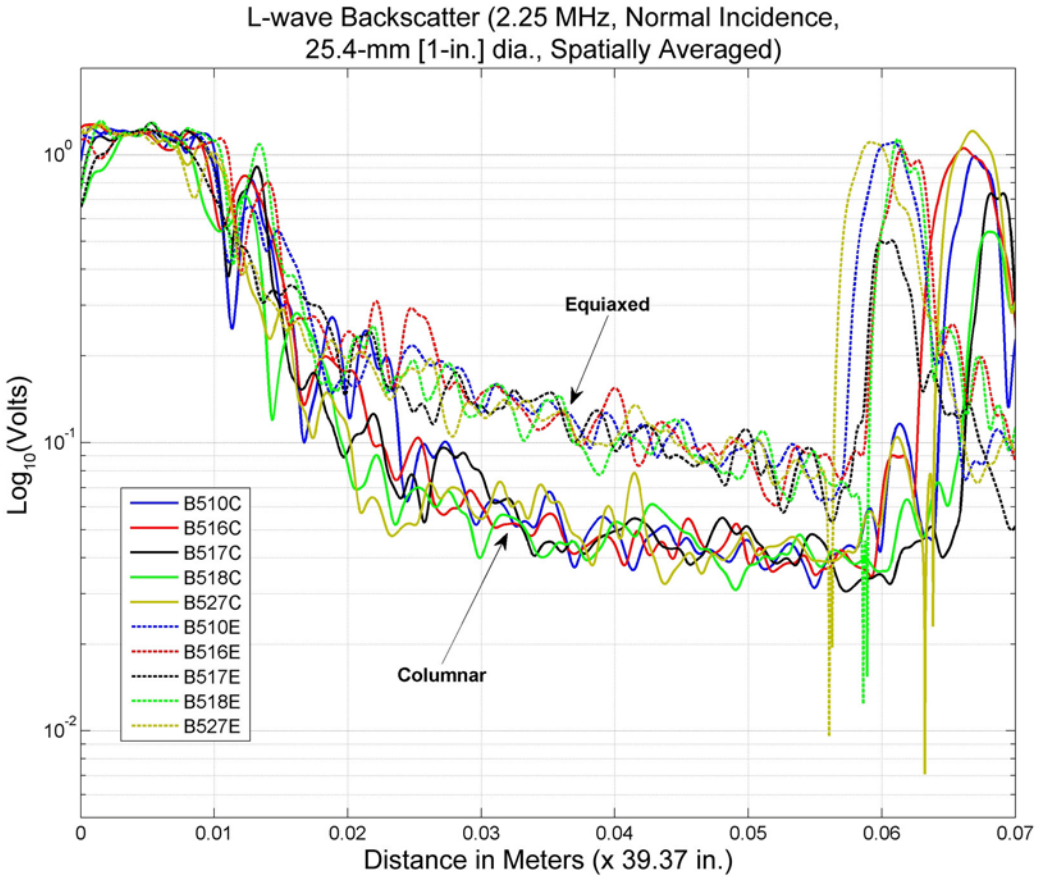

Figure 3.7. Backscattered Energy (logarithmic plot) After Spatial Averaging, from Five Columnar and Five Volumetric Regions. The horizontal axis shows distance in meters (assuming a nominal wave speed of 5800 m/s [2.28×10^5 in./s] in CASS). The front surface reflection is to the left, and the first back-surface reflection is seen at the extreme right of the plot.

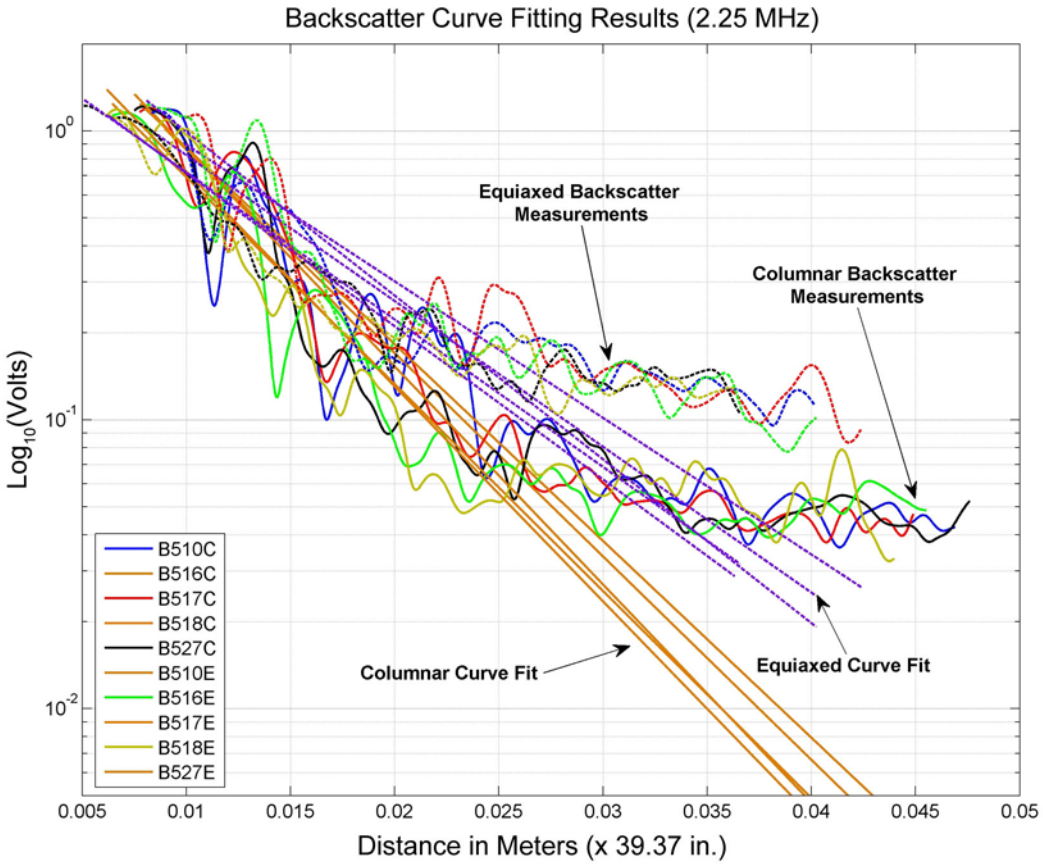

Figure 3.8. Exponential Curve Fitting to Backscattered Energy (plotted on a logarithmic scale). Backscattered energy from columnar regions is seen to decay faster while backscattered energy from equiaxed regions decays slower. In both cases, the backscattered energy deviates from a pure exponential decay (after about 2 cm (0.79 in.) into the material).

3.3 Acoustic Diffuse Fields

3.3.1 Diffuse Field Experimental Setup

The experimental setup for measuring ultrasonic diffuse fields is shown in Figure 3.9. The experimental setup used a HP arbitrary waveform generator (model 33120A), RITEC broadband receiver (model BR-640), RITEC diplexer (RDX-2), Panametrics ultrasonic preamplifiers (model 5660B), a LeCroy (LeCroy Corporation, Chestnut Ridge, New York) oscilloscope (model WaveRunner 64Xi), and two transducers in pitch-catch mode. The transmit transducer was a 6.35-mm (0.25-in.)-diameter KBA contact transducer with a center frequency of 2.25 MHz. The receive transducer was a Valpey-Fisher broadband microprobe with an effective bandwidth up to 2.5 MHz.

The two transducers were placed in contact with the outer surface of the specimen at a separation distance of 76.2 mm (3 in.), with a thin layer of ultrasonic gel couplant to ensure proper coupling of energy to the specimen. The arbitrary waveform generator was programmed to output a 500-mV, 6-cycle tone burst, with the operating frequency varied between 1.9 MHz and 2.2 MHz. The resulting tone burst was applied to the transmit transducer. The microprobe was used to record the resulting acoustic/material

interaction over a time period of 9.75 milliseconds. (Pre-trigger measurements corresponding to 0.25 ms were also collected, resulting in a total of 10 milliseconds of data.) The signal from the microprobe was amplified using the two preamplifiers in cascade (with a total gain of 100 dB), and 256 consecutive waveforms were averaged to minimize the effect of electronic noise. In addition, a low-pass filter with a cutoff frequency of 6.025 MHz was applied to remove any high-frequency noise. Because the highest frequency of the tone burst is 2.2 MHz (and the bandwidth of the microprobe is less than 3 MHz), it is unlikely that the low-pass filter impacts the useful signal component of the measurement. A LeCroy (model WaveRunner 64Xi) digital oscilloscope was used to perform the averaging and filtering, and to digitize and save the signals. The averaged signal was sampled at 250 MHz, and the samples saved and exported to the MATLAB software package (Version R2009b) for analysis.

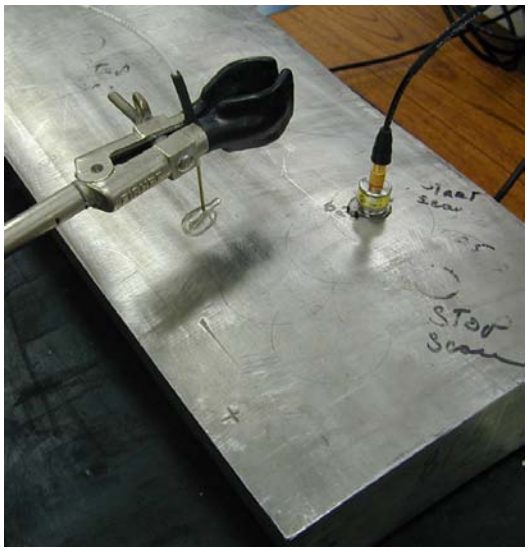

(a) Transducer and microprobe on CASS specimen

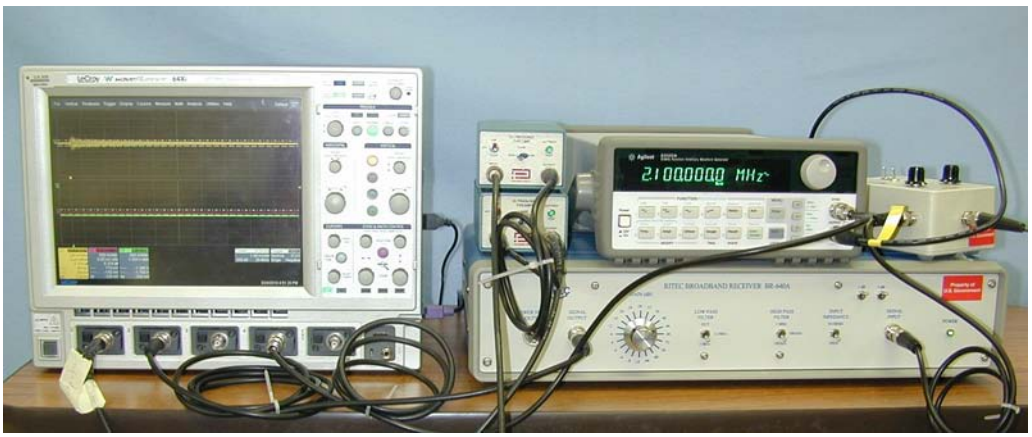

(b) Example of signal from CASS specimen

Figure 3.9. Instrumentation Used for Diffuse Field Experiment. Data were sampled at 250 MHz and exported to the MATLAB software for analysis.

In addition to the microprobe measurements, the pulse-echo signal from the transmit transducer was also recorded using the RITEC diplexer and receiver for future analysis. This measurement was also averaged (over 256 consecutive measurements), sampled at 250 MHz, and saved using the LeCroy oscilloscope. The instrument settings for the pulser, receiver, preamplifiers, and diplexer were held constant throughout the experiment. In particular, the tone-burst amplitude (500 mV) and the gain on the preamplifiers were held constant regardless of whether the material being inspected was columnar or equiaxed. This enables a direct comparison of the measurement data from each region.

3.3.2 Diffuse Field Data Analysis

Ultrasonic measurements from the five columnar and five equiaxed specimens (at a tone-burst frequency of 2.2 MHz) are presented in Figures 3.10 and 3.11. A visual comparison of the data indicates that the ultrasonic energy in equiaxed specimens decays faster than that in columnar specimens. (The large spike at the beginning of the signals is likely from trigger bleed-through, and was removed prior to analysis – see below.) This could be a manifestation of higher attenuation (and potentially higher diffuse field dissipation) in these microstructures. To enable a quantitative comparison, the following processing steps were used:

1. Signal Extraction: This step identified the location of the trigger, and truncated the measurement to remove the initial (pre-trigger and trigger bleed-through) section. This step used trigger information saved using the oscilloscope to determine the location of the trigger pulse.
2. Down-sampling: The resulting signal was down-sampled (Lyons 2004) by a factor of 10, effectively using every tenth sampled point and resulting in an effective sampling rate of 25 MHz. This step was applied due to limitations on available computer memory. Note that the highest frequency component of the measurement is under 3 MHz and, consequently, no information is lost from the down-sampling operation.
3. Energy Computation: The energy in the signal was extracted by squaring the measurement and low-pass filtering the result (Ramamoorthy et al. 2004). The cut-off frequency for the low-pass filter (Lyons 2004) was selected to be 12 kHz based on the stability of the energy data with respect to the cutoff frequency.
4. Parameter Estimation: The diffusivity and dissipation were estimated by approximating the specimen as a rectangular slab, and fitting Eqn. (2.1) to the measured energy data from Step 3 (Ramamoorthy et al. 2004). The unknown parameters were assumed to be the diffusivity D and dissipation σ. The specimen dimensions and the position of transmit and receive transducers were used in the curve-fitting procedure. The summations in the equation were truncated to 75 terms each (i.e., $n = 1,2,...,75$ and $m = 1,2,...,75$). A nonlinear least-squares minimization algorithm (Antoniou and Lu 2007) was used to fit the analytical function to the measured data and estimate the diffusivity and dissipation.
5. Frequency Analysis: Each step above was performed for data from each frequency. The resulting values of dissipation and diffusivity were used to extract the arrival time of the energy peak, as a function of frequency.

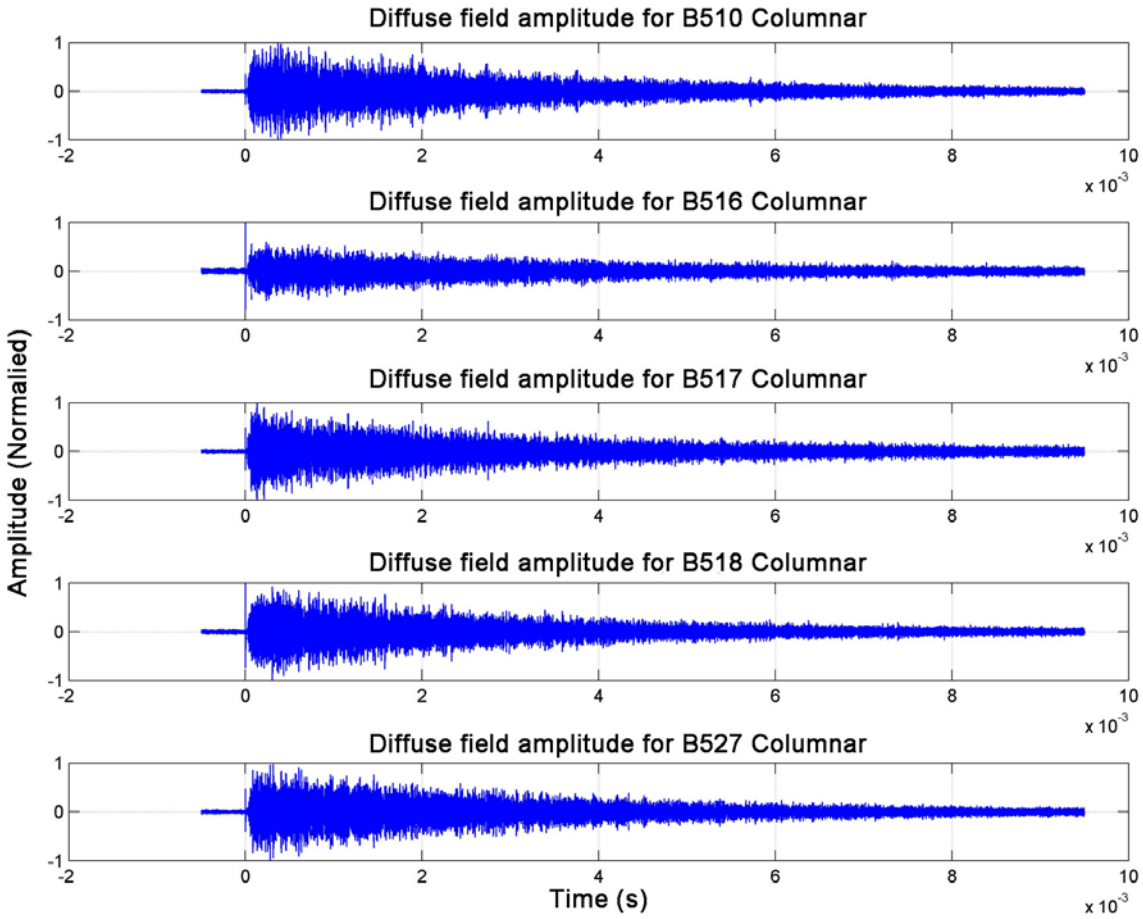

Figure 3.10. Ultrasonic Diffuse Field Measurements for Five Columnar Regions. The specimen was insonified using a tone-burst excitation at 2.2 MHz, and the resulting material-ultrasonic interaction was recorded using a microprobe.

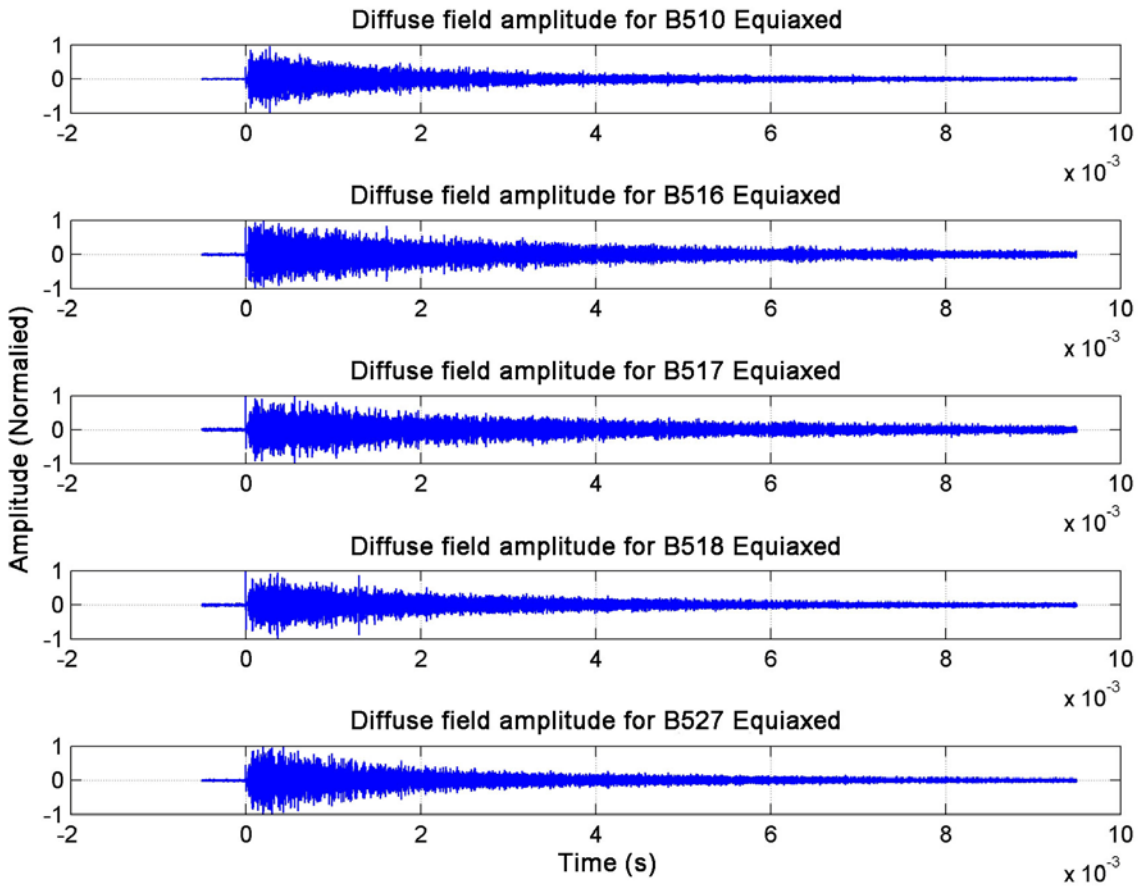

Figure 3.11. Ultrasonic Diffuse Field Measurements for Five Equiaxed Regions. The specimen was insonified using a tone-burst excitation at 2.2 MHz, and the resulting material-ultrasonic interaction was recorded using a microprobe.

3.3.3 Diffuse Field Results

Figure 3.12 shows an example of the analytical function fit to the experimental diffuse energy measurement. Data from one columnar and one equiaxed region (obtained at a tone-burst frequency of 2.2 MHz) are presented in the figure. Small differences in the peak arrival time are apparent, indicating a difference in the diffusivity and dissipation. Figure 3.13 shows the arrival time as a function of dissipation and diffusivity, for five columnar regions (stars) and five equiaxed regions (diamonds). The data are presented for four frequencies (1.9 MHz, 2.0 MHz, 2.1 MHz, and 2.2 MHz). The same information is also presented in tabular form in Table 3.1.

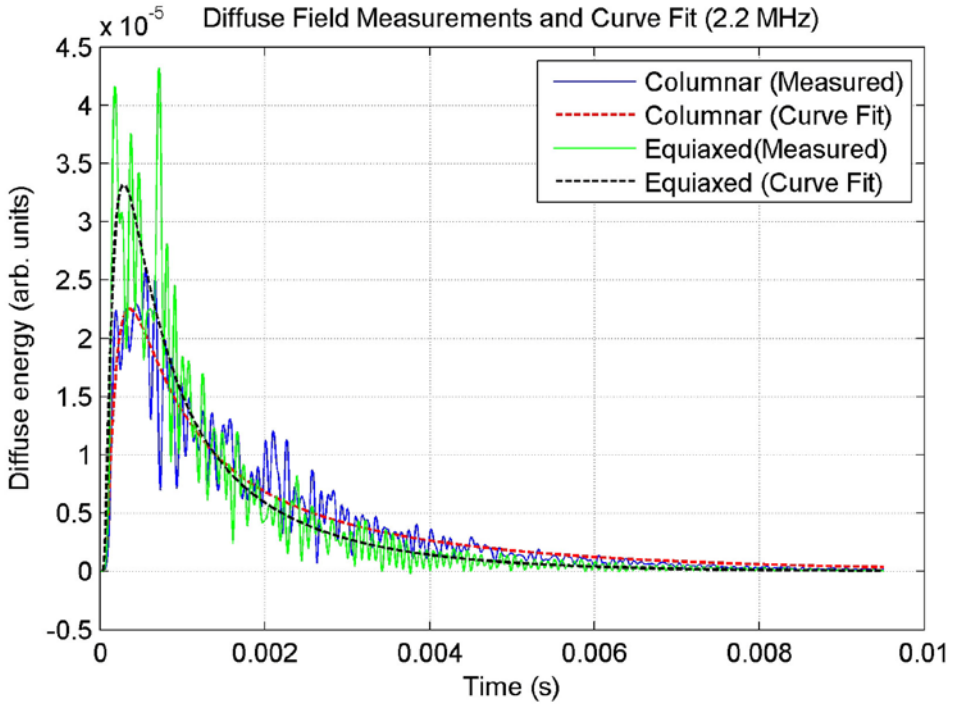

(a)

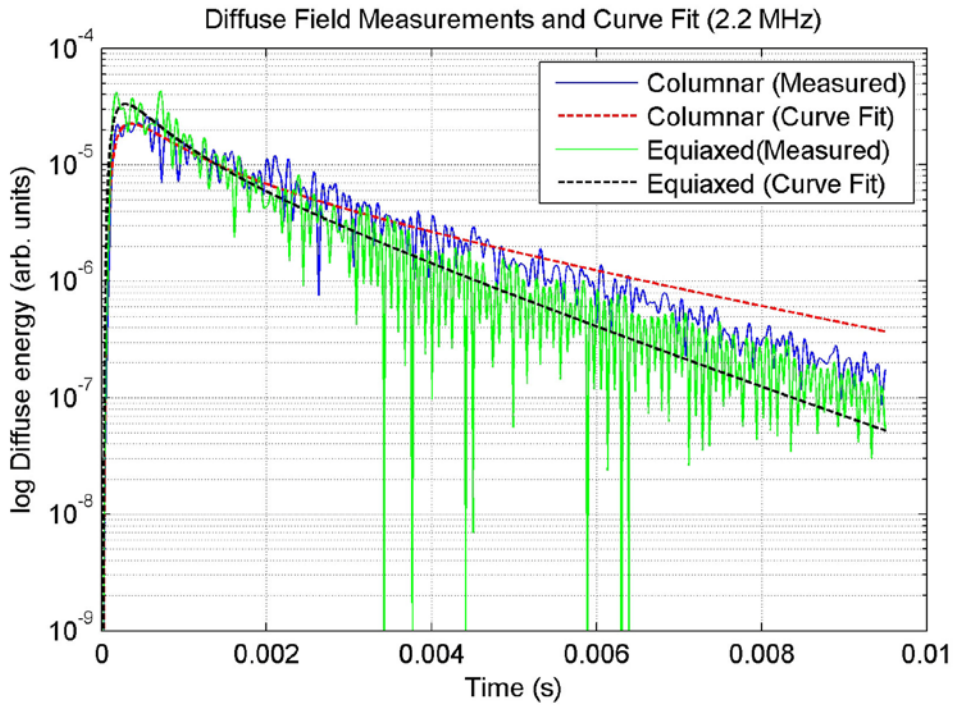

(b)

Figure 3.12. (a) Diffuse Energy Curve Fit Results. (b) Curve Fit Results Plotted Using a Logarithmic Scale. The measurement was obtained at 2.2 MHz.

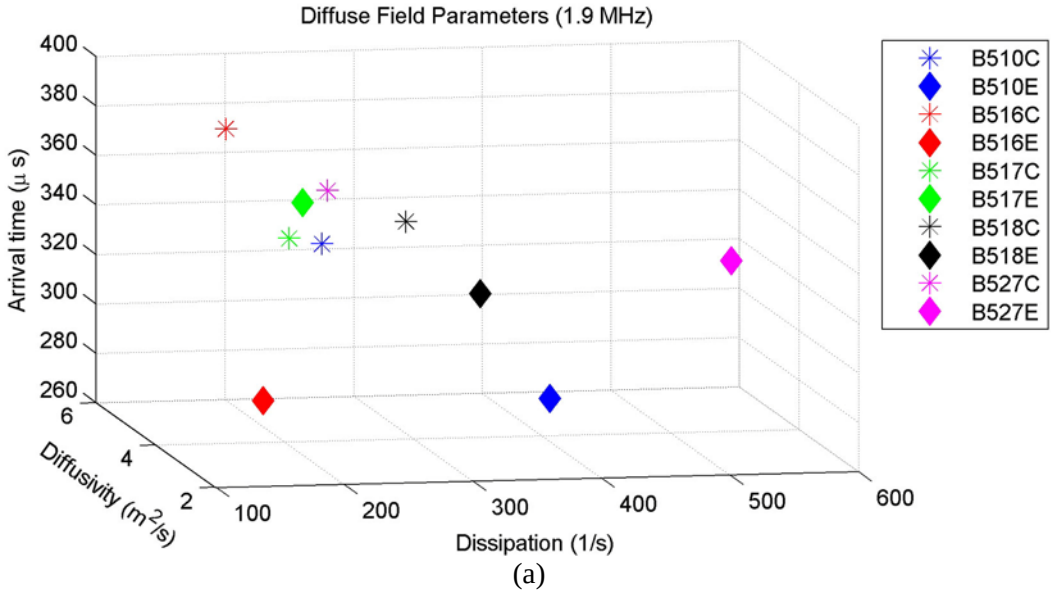

(a)

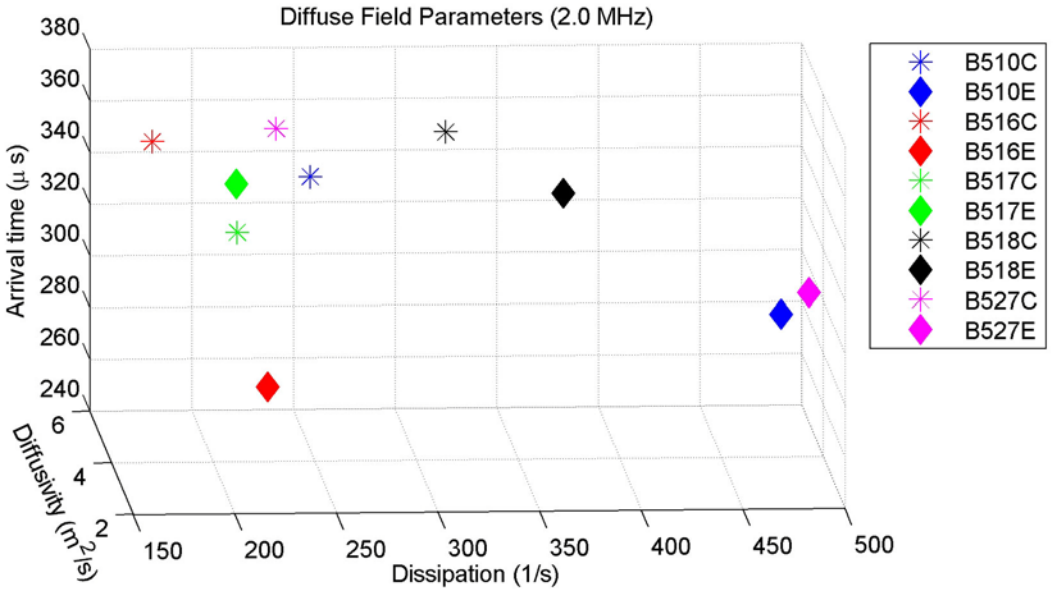

(b)

Figure 3.13. Arrival Time (in microseconds) Plotted as a Function of Dissipation and Diffusivity at a Tone-Burst Frequency of (a) 1.9 MHz, (b) 2.0 MHz, (c) 2.1 MHz, and (d) 2.2 MHz. The stars in the plots indicate measurements from columnar regions while the diamonds indicate measurements from equiaxed regions. The parameters from the different specimens are shown using different colors. Diffusivity may be converted to in.^{2}/s by multiplying by 1550.

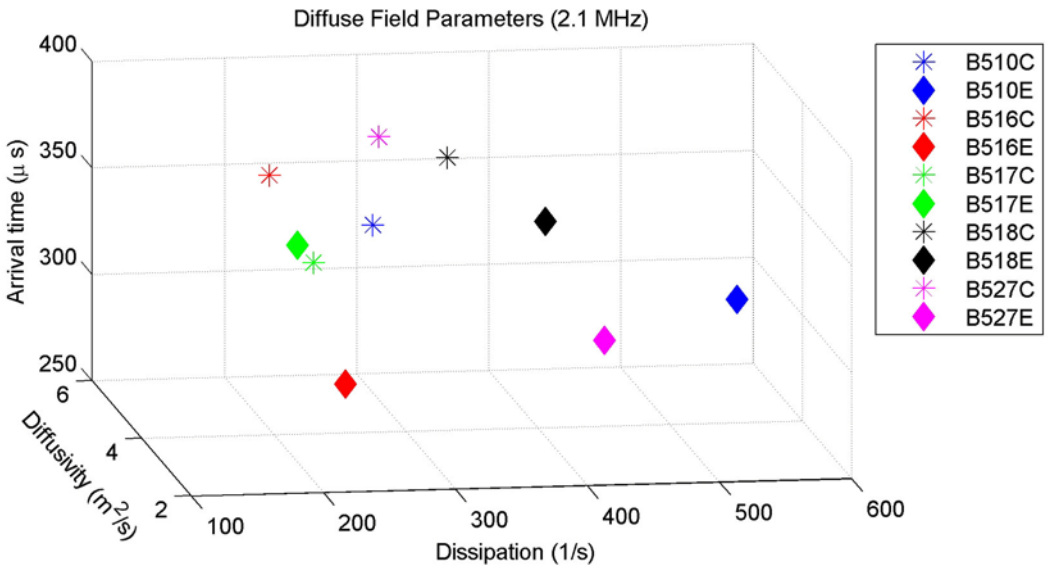

(c)

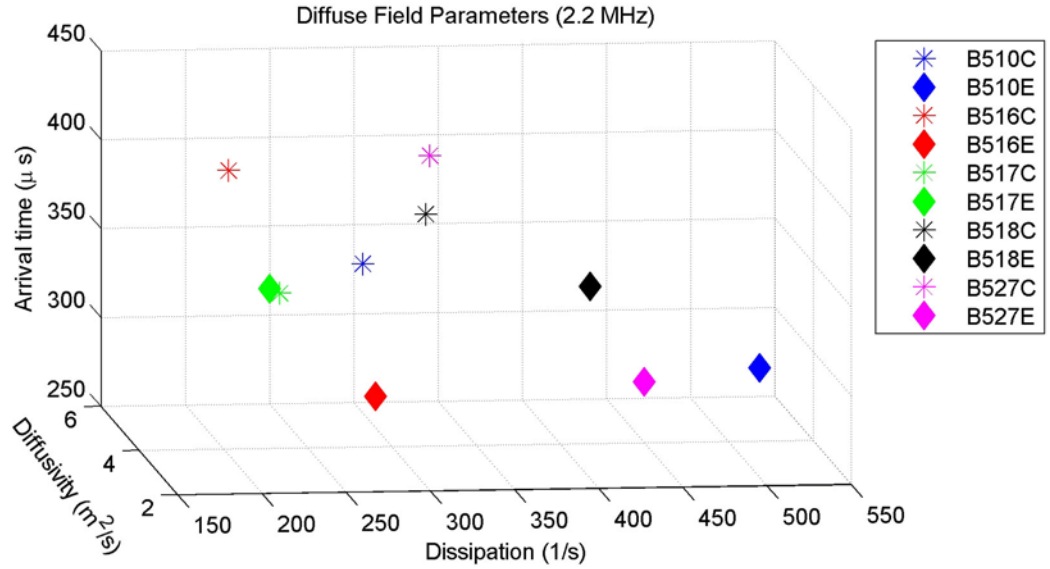

(d)

Figure 3.13 (continued)

Table 3.1. Arrival Time, Diffusivity, and Dissipation Tabulated as a Function of Frequency

Frequency (MHz)		1.9			2			2.1			2.2		
		Diffusivity (m^2/s)[(a)]	Dissipation (1/s)	Arrival Time (From Fit) (s)	Diffusivity (m^2/s)[(a)]	Dissipation (1/s)	Arrival Time (From Fit) (s)	Diffusivity (m^2/s)[(a)]	Dissipation (1/s)	Arrival Time (From Fit) (s)	Diffusivity (m^2/s)[(a)]	Dissipation (1/s)	Arrival Time (From Fit) (s)
Columnar	B510	3.960	228.009	3.402E-04	3.793	246.509	3.521E-04	3.785	270.756	3.503E-04	3.699	279.056	3.569E-04
	B516	3.511	143.108	3.915E-04	3.726	168.463	3.670E-04	3.589	188.796	3.776E-04	3.226	194.065	4.164E-04
	B517	3.961	202.729	3.427E-04	4.148	212.565	3.272E-04	4.101	231.760	3.289E-04	3.988	233.228	3.374E-04
	B518	3.766	289.144	3.500E-04	3.497	311.609	3.720E-04	3.336	318.858	3.873E-04	3.329	312.266	3.888E-04
	B527	3.684	226.264	3.641E-04	3.587	228.659	3.729E-04	3.294	266.321	3.984E-04	3.012	311.112	4.256E-04
Equiaxed	B510	4.877	426.720	2.672E-04	4.363	481.272	2.918E-04	4.036	551.309	3.076E-04	4.411	522.955	2.863E-04
	B516	5.154	210.405	2.667E-04	5.369	234.183	2.551E-04	5.318	278.911	2.548E-04	5.070	302.535	2.650E-04
	B517	3.763	208.580	3.589E-04	3.877	210.712	3.488E-04	3.988	217.789	3.390E-04	3.958	226.738	3.405E-04
	B518	4.116	355.112	3.170E-04	3.722	370.742	3.457E-04	3.614	398.418	3.523E-04	3.717	414.399	3.421E-04
	B527	3.713	540.841	3.316E-04	4.189	494.063	3.016E-04	4.536	460.429	2.831E-04	4.669	457.592	2.760E-04

(a) Diffusivity can be converted to $in.^2/s$ by multiplying by 1550.

3.4 Discussion

Longitudinal-wave backscatter and diffuse field measurements appear to have the potential to classify CASS material as equiaxed-grain or columnar-grain material. Data showed moderate scatter; however, equiaxed-grain material exhibited higher backscatter than columnar-grain material at 2.25 MHz. The backscatter measurements also indicated a strong propensity towards multiple scattering at 2.25 MHz. There is, therefore, a likelihood that the multiple scattering measurement can be used to determine the scattering coefficient (Goebbels 1980, 1994), either with a single measurement or measurements at multiple frequencies.

A preliminary analysis of data from the purely columnar specimens indicated higher scattering in the outer 1–2 cm (0.39–0.79 in.) of the specimen, and a potential inhomogeneity (identified by a strong backscatter peak) at approximately 1–2 cm from the outer surface. This appears to be consistent with microstructural studies reported in Ramuhalli et al. (2009) showing an approximately 1-cm (0.39-in.) band of randomly oriented grains after which the dominant columnar grain structure developed. However, this needs confirmation from additional studies using layered microstructures. Note that the thickness of the band can vary depending on the extent of outer surface machining of the original casting.

Backscatter measurements at 1 MHz were also obtained on a subset of the specimens. These backscatter measurements at 1 MHz, however, did not show any significant differences between the two microstructure categories. This is likely due to the grain sizes in the CCSS specimens that were chosen for this study. All of these specimens were created by welding two (large-diameter) pipes (one with equiaxed grains and the other with columnar grains), and then sectioning the resulting weld region. One specimen (B515) from this set was destructively analyzed and the grain sizes recorded. The minimum columnar grain size was 0.6 mm (0.02 in.) while the maximum was 12 mm (0.47 in.). Similarly, the minimum and maximum equiaxed grain sizes were 0.6 mm (0.02 in.) and 7 mm (0.28 in.), respectively (Anderson et al. 2007). The mean lineal intercepts (which are proportional to the equivalent diameter of a spherical grain) of this specimen are 2.34 mm (0.092 in.) (equiaxed) and 2.48 mm (0.097 in.) (columnar). Assuming that these grain sizes are representative of the specimens used in this study, and using a wavelength of 2.58 mm (0.102 in.) (at 2.25 MHz, in stainless steel), the ratio of mean grain size-to-wavelength d/λ is between 0.9 and 1. Scattering is therefore firmly within the stochastic regime, and strong multiple scattering is a possibility. However, at 1 MHz, the wavelength in stainless steel is 5.8 mm (0.23 in.), resulting in $d/\lambda \approx 0.4$. Thus, it is likely that the material appears to be somewhat homogeneous at this frequency. The result is potential scattering behavior closer to the Rayleigh regime. While some multiple scattering may occur at 1 MHz in these specimens, the dominant scattering behavior is likely to resemble single scattering, with very little difference in the scattering behavior between the two microstructures. Further, note that the specimen thickness is close to an integral multiple of the wavelength at 1 MHz, and therefore this frequency may be close to a resonant frequency of the specimens examined. This may also affect the backscatter measurements at this frequency, given that attenuation in these specimens (Ramuhalli et al. 2009) at 1 MHz was somewhat low.

The diffuse field measurements also show potential for discriminating between the different microstructures. As seen from the data, measurements from equiaxed specimens have generally higher diffusivity and higher dissipation, and faster arrival times when compared to the data from columnar regions. Again, this is likely indicative of the random orientation of grains in equiaxed microstructures, resulting in more uniform mode conversion to shear modes in all directions and greater dissipation as a result. Note that the dissipation is generally expected to increase with frequency (Punurai et al. 2007)

(because absorption and attenuation increase with frequency). The dissipation factors estimated from the measurements show this trend in most of the specimens examined. Similarly, diffusivity is generally expected to reduce with increasing frequency. Again, the diffusivity estimates are seen to trend in the anticipated direction for most specimens.

Data from one equiaxed specimen (B517) were not within the expected range of equiaxed measurements. There is also some variability in the estimated diffuse field parameters, as seen from Figure 3.13. There are three potential reasons for these observations. The first is potential variations in the microprobe contact with the specimen, which will result in variability in the measurements. Overcoming these issues will require the design of mechanical fixtures that can ensure consistent coupling of the microprobe in an in-situ setting. The second possibility is that the approximation inherent in Eq. (2.1) results in parameter estimates that are not very accurate. Addressing this issue will require the development of more accurate models that represent the ultrasonic diffusion process in CASS materials. The use of procedures to determine the variance in the estimated parameters (Weaver 1998) will also help determine the accuracy in the diffuse field parameter estimates and determine whether the observed trending in the parameters (as a function of frequency) is accurate.

The third possible reason for the variability in the diffuse field parameters (and particularly the anomalous measurement from the equiaxed side of B517) is the presence of flaws within the specimen. Because the diffuse field measurement is statistically sampling the entire volume of the specimen, the presence of flaws (especially cracks) will alter the response. This is particularly true when the flaw is between the transmitter and receiver (Ramamoorthy et al. 2004). The result in this case is a delayed arrival of the diffuse field energy peak. Examination of specimen B517 showed more than one pinhole-sized surface anomaly on both the inner and outer surface as well as at least one flat-bottom hole machined on the inner surface. While other specimens (such as B527) also have pin-hole sized surface anomalies, none of the specimens used in the diffuse field measurements had larger sized machined flaws in the base material. It is possible that the machined flaws in B517 are large enough to interact significantly with the diffuse ultrasonic energy. The resulting behavior of late arrival time and lower dissipation/diffusivity will mimic columnar microstructural behavior, and additional measurements (for instance, at significantly different frequencies or at different locations) may be necessary to resolve the issue.

Acoustic wave propagation in equiaxed-grain materials also depends on the texture and related degree of anisotropy (Papadakis 1965; Hudgell and Gray 1985). The metallographic characterization reported in Ramuhalli et al. (2009) indicated a preferred direction for the dendritic colonies in the equiaxed region. Such preferred orientation will impact scattering and energy diffusion. It is unknown at this time how this may impact the discrimination capability of these acoustic measurement methods.

Several variables used in the calculations (such as the phase velocity used to estimate the acoustic path length in backscattering, and the specimen dimensions used in the diffuse field calculations) may not be known precisely in a field setting. Some experimental variables such as the ultrasonic coupling must also be controlled carefully to obtain reliable measurements of backscatter and diffuse field energy. Finally, it may be more useful in a field setting to compute backscattering and diffuse energy parameters relative to known microstructures to enable in-situ classification of grain structure.

4.0 An Evaluation of Potential Electromagnetic In-situ Characterization Methods

This section describes preliminary experiments and results of applying eddy current measurements to the CASS microstructure characterization problem. As with ultrasonic methods discussed in the previous section, a two-class discriminant problem was postulated here (either equiaxed-grain or columnar-grain CASS material). Details of the eddy current measurements for microstructure characterization are provided in this section.

4.1 Centrifugally CASS Specimens

Seven specimens were used for the evaluation of eddy current-based microstructure characterization. Four of these specimens (B510, B517, B518, and B27) were those described in Section 3.1. In addition, specimens B508, B511, and B528, also part of the PISC-III specimens and containing similar microstructure as the other four, were included in the evaluation.

4.2 Multi-frequency Eddy Current Measurements

4.2.1 Experimental Setup

The experimental setup used a Nortec (Olympus NDT, Inc., Waltham, Massachusetts) eddy current instrument (model 500D) with a 15.75 mm (0.62-in.)-diameter absolute probe (Figure 4.1). The rated operating frequency of the probe was between 300 Hz and 10 kHz. While excitation frequencies outside this frequency band can be used with the probe, the probe response will first need to be calibrated using reference standards. A mechanical scanner was used to scan a (approximately) 50.8-mm × 12.7-mm (2-in. × 0.5-in.) region on the outer surface of the specimen with a spatial resolution of 0.102 mm × 0.076 mm (0.004 in. × 0.003 in.). The region scanned was selected to ensure that the probe was perpendicular to the specimen surface over the entire scan region. Three excitation frequencies were selected for this initial study – 1 kHz, 10 kHz, and 25 kHz, to ensure that effects of variation in microstructure as a function of depth were captured in the measurement.

Because the permeability is variable, a calibration procedure was used to normalize the recorded responses. For each excitation frequency, the probe, after being balanced in air, was placed over a calibrated ferrite specimen (Figure 4.2). The probe liftoff signal was rotated until it was set at 0 degrees (corresponding to the negative horizontal axis). The gain on the instrument was set to ensure that the eddy current response from the calibration standard was full-scale, and the gain and rotation settings were recorded. The calibration process also ensured that the measurement at 25 kHz can be compared to the measurements at 1 kHz and 10 kHz.

Data acquisition used a desktop computer with a National Instruments A/D card and associated data acquisition software. The sampling rate was set to 125 Hz, and the real and imaginary (horizontal and vertical) components of the complex eddy current probe response were recorded. The data was then transferred to the MATLAB software (version R2009b) for further analysis.

Figure 4.1. Eddy Current Scan Setup

Figure 4.2. Commercially Procured Ferrite Calibration Standard. The base standard (left) has a ferrite content of 104%, while the other three have ferrite levels of 2.87%, 10.7%, and 33.5%.

4.2.2 Eddy Current Data Analysis

The eddy current measurements were analyzed using the following procedure:

1. Gain Calibration: The measurement at each frequency was scaled to a standard gain value (62.8 dB) to enable comparison across frequencies. If the original gain setting was g_1 dB (on both the horizontal and vertical channels), then the rescaling was achieved by multiplying the measurement by a scaling factor S given by

$$S = 10^{\left(\frac{62.8 - g_1}{20}\right)} \tag{4.1}$$

2. Phase Calibration: The phase rotation prior to data acquisition ensured that the measurement at each frequency was acquired using a standardized setting. However, this process removes information about phase changes as a function of frequency. This step rotated the data back (using the stored rotation information from the data acquisition step) to recreate the relative phase change as a function of frequency.

3. Magnitude and Phase Computation: The magnitude and phase angle at every scan location, for each frequency, were computed using the data from step 2.

4. Feature Computation: The change in magnitude and phase as a function of frequency was computed at each measurement location within the scan region. Specifically, the change in magnitude was computed as ratios (the ratio of the magnitude at 10 kHz to the magnitude at 1 kHz, and the ratio of the magnitude at 25 kHz to the magnitude at 10 kHz). The change in phase angle was computed as the difference in phase between 10 kHz and 1 kHz, and between 25 kHz and 10 kHz at each measurement location. The average and standard deviation (over the scan region) of the magnitude ratio, and the average and standard deviation (over the scan region) of the phase change, were then computed. These features were examined for correlations with microstructure.

4.2.3 Results and Discussion

Figure 4.3 presents examples of the eddy current C-scans (at 1 kHz) for equiaxed and columnar regions. The axes on the plot represent the axial and circumferential directions. Figure 4.4 shows the individual data values in the impedance plane (magnitude and phase) for a columnar and equiaxed region. From these scans, the average measurement within the scan region and the standard deviation within the scan region were computed. This information, for each frequency and region, is shown in Figure 4.5. The plot presents the average impedance and standard deviation, with the resistive and reactive components for seven specimens shown as a function of frequency. In the figure, the different colors represent the different specimens, while the symbols represent measurements from columnar and equiaxed microstructures at three different frequencies. The standard deviation (in the resistive and reactive components) is represented by horizontal and vertical lines at each marker location. As seen from this figure, consistent magnitude and phase differences are not apparent between the columnar and equiaxed regions. Therefore, using the magnitude or phase measurements directly to determine microstructure appears to be a difficult proposition.

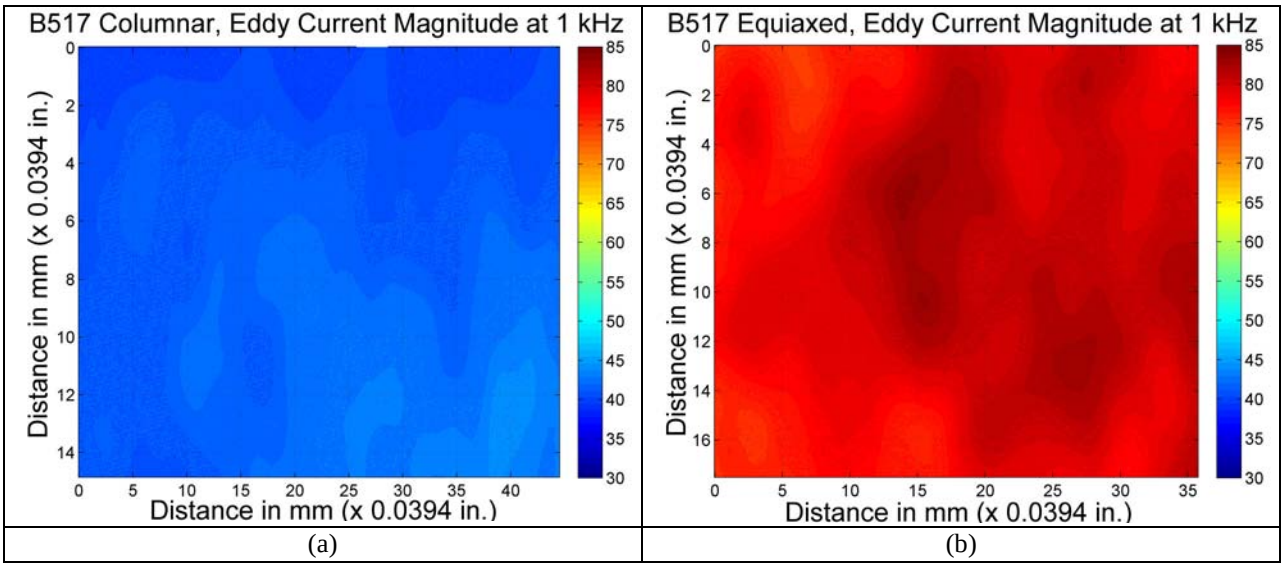

Figure 4.3. Eddy Current Magnitude for (a) a Columnar, (b) an Equiaxed Region. The excitation frequency is 1 kHz, and the data were acquired on the outer surface of the specimen.

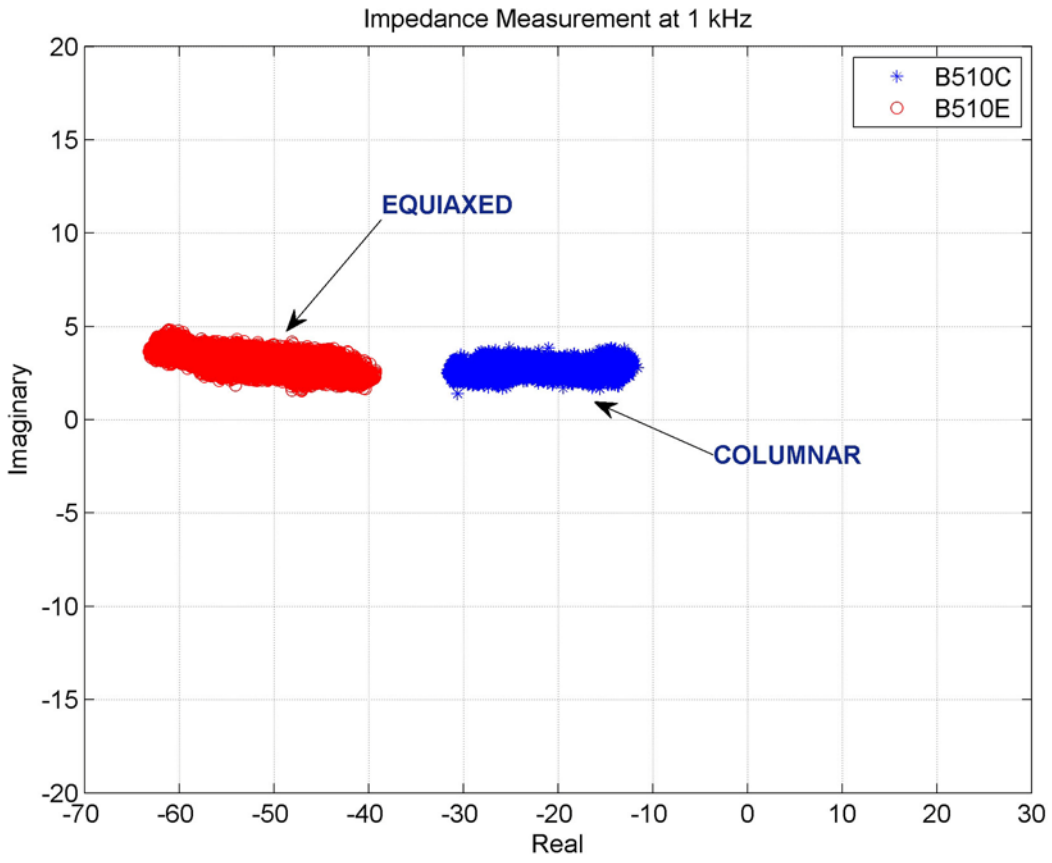

Figure 4.4. Impedance Plane Plot of Eddy Current Measurements (at 1 kHz) from Columnar and Equiaxed Regions

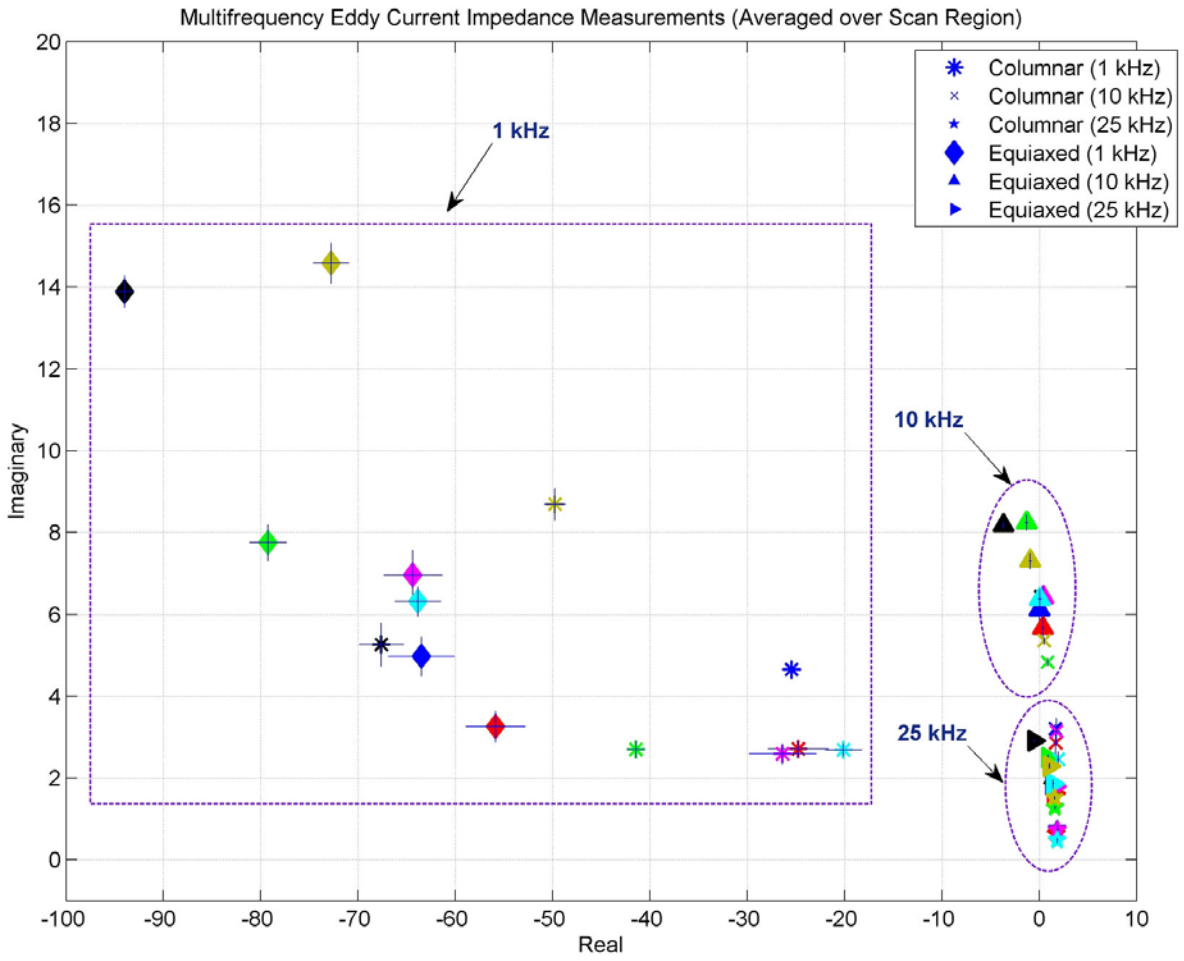

Figure 4.5. Eddy Current Measurement Variation as a Function of Frequency

Figure 4.6 presents the change in magnitude and phase with frequency. Note that the standard deviation (shown in Figure 4.6 as horizontal and vertical lines, centered on each marker) in most instances is rather low. When the fractional change (ratio) in magnitude with frequency is examined (Figure 4.6a), it is apparent that columnar regions, in general, have smaller changes in magnitude with frequency (resulting in larger magnitude ratios). This is likely due to two factors. First, the overall ferrite content in columnar regions is smaller than that in equiaxed regions. Second, the ferrite content tends to vary through the thickness of the specimen (in both equiaxed and columnar regions), resulting in a variable magnetic permeability over the specimen thickness. Measurements suggested that, in columnar microstructures, the ferrite content (and therefore permeability) increases from the outer surface to the inner surface. In contrast, in equiaxed regions, the ferrite level either decreases from outer to inner surface, or is (somewhat) constant.

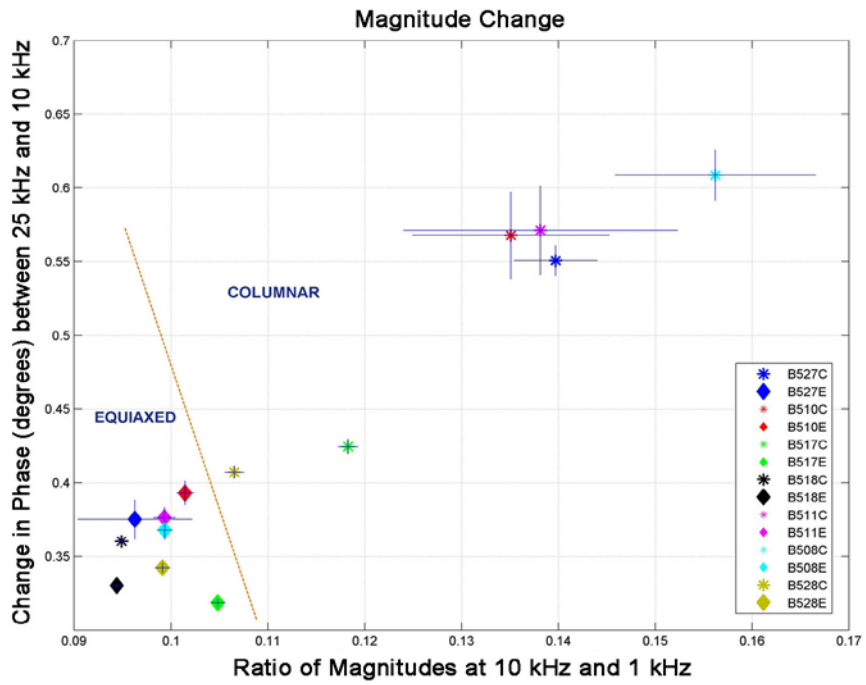

(a)

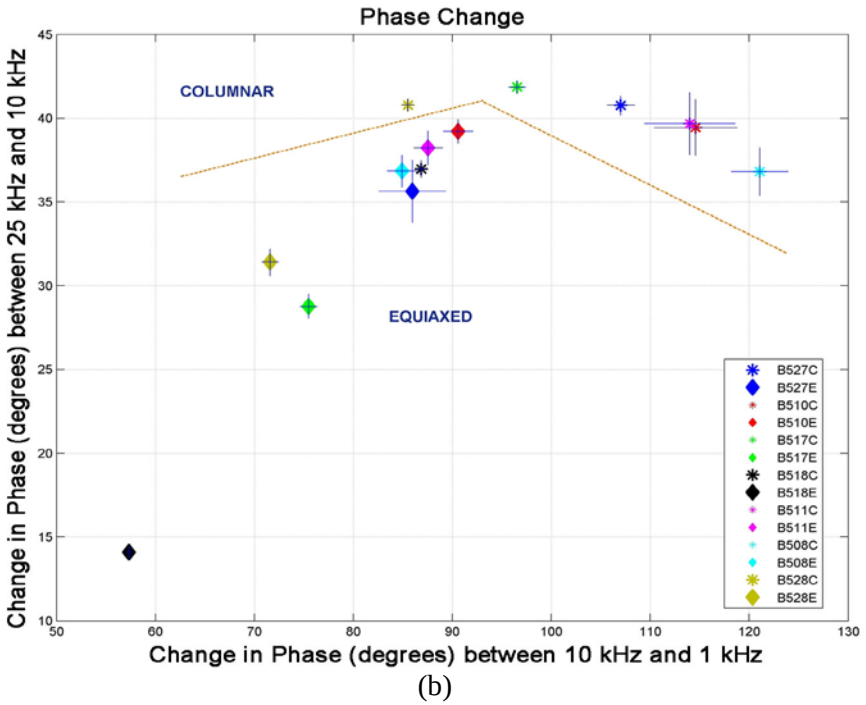

(b)

Figure 4.6. (a) Average Fractional Change in Magnitude and (b) Average Change in Phase as a Function of Frequency. The horizontal axis in both (a) and (b) represents the change between measurements at 1 kHz and 10 kHz, while the vertical axis represents change between 10 kHz and 25 kHz. The standard deviation is represented by horizontal and vertical lines at each marker location.

Increasing the frequency results in a smaller depth of penetration of eddy currents and a correspondingly smaller volume where material–eddy current interactions take place. This in turn reduces the eddy current magnitude as the frequency increases. (The fact that permeability itself is variable as a function of depth results in additional changes in the skin depth that are generally difficult to quantify analytically.) The higher permeability of equiaxed regions will result in a smaller depth of penetration (compared to columnar regions) as the frequency increases. The result is that in equiaxed materials, the eddy current magnitude decreases by a larger factor as the frequency increases (resulting in smaller ratios).

As the frequency increases, the decrease in skin depth will result in an increase in resistance and a decrease in inductance of the eddy current probe. The result, in addition to a change in magnitude, is also a change in phase. For materials with higher permeability, the decrease in inductance is smaller when compared to materials with lower permeability. The change in phase angle is therefore smaller for materials with higher permeability. An examination of Figure 4.6b shows that the phase change (with frequency) in equiaxed materials is lower than that of columnar materials. However, the variability demonstrated over several specimens makes the characterization of microstructure using this feature difficult.

The measurements demonstrate the impact of frequency and permeability on eddy current data. As seen from the results, for the same region, the measured magnitude and phase change significantly with frequency. When compared across regions, it is apparent that the columnar regions generally show lower responses (and greater phase values). This is likely due to their lower ferrite levels. Note, however, that the ferrite levels can vary within a class (and even within a region). Further, the presence of mixed microstructures (particularly layered microstructures) can impact the eddy current measurement. This is especially true as the frequency is increased, because the resulting response is affected by fewer layers and the response behaves as that from a single microstructure. Thus, it is unlikely that the raw (absolute) eddy current measurement can be used as the sole microstructural classification feature, and therefore, additional measurements (or measurements from reference microstructures) may be necessary to achieve the goal of microstructure characterization. Examination of the magnitude maps from individual scans also raises the possibility that image analysis tools can potentially be used to extract key attributes of the measurements (such as the spatial variation in eddy current magnitude and phase) that potentially contain discriminatory information for microstructure characterization. This approach requires further evaluation.

5.0 Conclusions and Recommendations

This document summarizes a proof-of-concept study of in-situ ultrasonic and electromagnetic methods for classification and/or characterization of material microstructures in cast austenitic stainless steel (CASS) components from the outside surface of a pipe. The results demonstrated the potential of ultrasonic measurements to classify the material type of CASS for two consistent microstructures. Given the simple two-class problem of material being either equiaxed-grain material or a columnar-grain material, both normal incidence longitudinal-wave backscatter and diffuse field measurements appear to provide a reliable means to correctly classify material type. The backscattering measurements and a threshold algorithm classified all 10 material samples correctly and indicated a potentially reliable and robust technique. Attributes computed from the diffuse field measurements, along with a threshold algorithm, classified 9 out of 10 samples correctly. The cause for the misclassification of an equiaxed specimen as columnar needs further investigation, although it is believed that this error is due to changes in the diffuse field distribution from the presence of internal flaws/voids. The experiments provided promising results and demonstrated that there is a good basis to believe that potential exists for further development of these techniques for real-time in-situ classification of CASS material.

For the same two-class problem, average magnitude and average phase changes as a function of frequency from multi-frequency eddy current measurements also showed potential for microstructure classification. Relative changes in magnitude and phase at three frequencies correctly classified 13 out of 14 material samples. However, the eddy current method is limited in its applicability due to the skin effect, and very low excitation frequencies may be necessary to inspect and characterize typical thick-section CASS components currently used in nuclear power plants.

One advantage to ultrasonic backscatter measurements is the potential for microstructure classification as a function of thickness. A preliminary analysis of data from the purely columnar specimens indicated higher scattering in the outer 1–2 cm of the specimen. This appears to be consistent with microstructural studies reported in Ramuhalli et al. (2009) showing an approximately 1-cm band of randomly oriented grains after which the dominant columnar grain structure develops. However, this needs confirmation from additional studies using layered microstructures.

The diffuse field measurements are an average over the material volume; therefore, a characterization as a function of time or depth may not be possible. Further, the measurements were seen to be sensitive to transducer positioning and coupling, and robust mechanical fixtures capable of providing consistent transducer placement and coupling will need to be created if this technique is to be used in the field. The accuracy of the diffuse field parameter estimates can be potentially improved with the use of accurate models that describe the ultrasonic diffusion phenomenon. The measurements also hinted at the ability of diffuse field measurements to identify the presence of flaws in the specimen. However, further studies in CASS specimens with and without flaws are needed to confirm this.

A potential issue with the use of ultrasonic techniques for microstructure characterization is the selection of an appropriate frequency. Frequency selection for microstructure characterization must ensure that the ultrasonic wave has significant measurable interactions with the microstructure. In most cases, this requires the selection of higher frequencies (shorter wavelengths) to ensure that significant multiple scattering occurs. In this respect, the requirements are opposite those of inspection for flaw detection, where the goal is minimal interaction of the ultrasonic wave with the microstructure. In

practice, because the grain sizes are unknown, it is likely that multiple frequencies will need to be used for in-situ characterization. A similar discussion holds for the selection of excitation frequency in electromagnetic methods for microstructure characterization. This choice will depend on the specimen thickness, ferrite content and permeability, and the microstructural class (pure or mixed, columnar or equiaxed). Because these quantities are not known a priori, a range of electromagnetic excitation frequencies will need to be selected for in-situ characterization.

It is unlikely that a single microstructural characterization method will be successful in an in-situ application due to the diverse nature of CASS microstructures and unknown parameters (such as grain size, wall thickness, etc.). An examination of the results obtained in this study shows that the misclassifications (using diffuse field and eddy current techniques) are on different samples. The misclassifications are likely due to different reasons. Thus, by combining information from multiple measurement methods, higher accuracy in microstructure characterization may potentially be achievable. Therefore, it may be necessary to use multiple measurement methods (both ultrasonic and electromagnetic) to achieve the goal of effective and reliable in-situ microstructure characterization.

In developing this investigation further into potential classification techniques of microstructure using in-situ measurements on CASS, work will focus on refining ultrasonic and electromagnetic measurement protocols, and conducting proof-of-concept experiments for other techniques that can be used to characterize inhomogeneous and anisotropic material. Continuing work includes:

- Verifying repeatability of the experiments, and confirming the results using additional specimens that are representative of the columnar- and equiaxed-grain structure (as well as mixed-grain structures). The microstructures selected will need to be representative of the majority of microstructures that can be encountered in legacy U.S. nuclear power plant components. However, the microstructures that may be encountered in legacy U.S. nuclear power plant components are generally not known, and an iterative process (iterating between microstructure characterization and improvement of the characterization tools) will probably be necessary for assembling a representative specimen set.
- Enhancing diffuse field measurements through more effective coupling, increasing the accuracy of parameter estimates through the use of accurate models of the ultrasonic diffusion phenomenon, and evaluating diffuse field behavior as a function of separation distance between the transmit and receive transducers, as a function of frequency. The use of accurate models of ultrasonic diffusion will be investigated in collaboration with ongoing theoretical modeling and simulation work conducted by Dr. Salahuddin Ahmed.
- Enhancing acoustic backscatter estimates by investigating scattering as a function of incident and receive angle, shear-wave backscatter measurements, computing scattering coefficient estimates over a broader frequency range through the use of broadband transducers employing swept frequency excitation, and correlating the backscattered energy to microstructural variation as a function of thickness. The need for diffraction correction to improve the accuracy of scattering coefficient calculations will also be investigated.
- Conducting shear-wave birefringence measurements to determine its applicability to the CASS microstructure classification problem.
- Evaluating other ultrasonic and electromagnetic methods used for microstructure and material characterization in other applications, which can be leveraged and applied to the CASS microstructural characterization challenge.

- Evaluating algorithms for assessing microstructural parameters (such as mean grain size and acoustic impedance variations within the material volume of interest) from one or more measurement types.
- Assessing the applicability of these techniques to characterizing cast primary circuit components (safe ends, elbows, or pipes) through inspection from the inner-diameter surface. According to ASME Code requirements, inspections from the inner diameter need only inspect the inner 1/3 of the wall. The techniques evaluated in this report (particularly the backscatter and eddy current measurements) can potentially provide better depth resolution and microstructure characterization in the required volume.

6.0 References

Anderson MT, SL Crawford, SE Cumblidge, KM Denslow, AA Diaz and SR Doctor. 2007. *Assessment of Crack Detection in Heavy-Walled Cast Stainless Steel Piping Welds Using Advanced Low-Frequency Ultrasonic Methods*. NUREG/CR-6933, PNNL-16292, U.S. Nuclear Regulatory Commission, Washington, D.C.

Antoniou A and W-S Lu. 2007. *Practical Optimization*. Springer, New York.

ASNT. 2004. *Nondestructive Testing Handbook, Third Edition: Volume 5, Electromagnetic Testing*. SS Udpa and PO Moore, American Society for Nondestructive Testing, Columbus, Ohio.

Auld BA. 1973. *Acoustic Fields and Waves in Solids, Volume 1*. John Wiley & Sons, New York.

Barat P, S De and SK Bandyopadhyay. 1998. "Fractal Property of Backscattered Acoustic Signals from Polycrystalline Aluminium." *Physics Letters A* 245(1–2):91–96.

Bates DJ, SR Doctor, PG Heasler and E Burck. 1987. *Stainless Steel Round Robin Test: Centrifugally Cast Stainless Steel Screening Phase*. NUREG/CR-4970, PNL-6266, PISC III Report No. 3, U.S. Nuclear Regulatory Commission, Washington, D.C.

Becker J, LJ Jacobs and J Qu. 2003. "Characterization of Cement-Based Materials Using Diffuse Ultrasound." *Journal of Engineering Mechanics* 129(12):1478–1484.

Bordier JM, M Fink, A Le Brun and F Cohen-Tenoudji. 1991. "The Influence of Multiple Scattering in Incoherent Inspection of Coarse Grain Stainless Steel." In *Proceedings of the 1991 IEEE Ultrasonics Symposium*, pp. 803-808. December 8–11, 1991, Orlando, Florida. Institute of Electrical and Electronics Engineers, IEEE Press, New York.

Chassignole B, O Dupond, L Doudet, V Duwig and N Etchegaray. 2008. "Ultrasonic Examination of an Austenitic Weld: Illustration of the Disturbances of the Ultrasonic Beam." In *Review of Quantitative Nondestructive Evaluation, Vol. 28*, pp. 1886–1893. July 20–25, 2008, Chicago. American Institute of Physics, Melville, New York.

Chassignole B, V Duwig, MA Ploix, P Guy and R El Guerjouma. 2009. "Modelling the Attenuation in the ATHENA Finite Elements Code for the Ultrasonic Testing of Austenitic Stainless Steel Welds." *Ultrasonics* 49(8):653–658.

Chatillon S, G Cattiaux, M Serre and O Roy. 2000. "Ultrasonic Non-Destructive Testing of Pieces of Complex Geometry with a Flexible Phased Array Transducer." *Ultrasonics* 38(1–8):131–134.

Connolly GD, MJS Lowe, SI Rokhlin and JAG Temple. 2008a. "Modeling the Propagation of Elastic Waves in Generally Anisotropic Materials and Austenitic Steel Welds." In *Review of Progress in Quantitative Nondestructive Evaluation, 34th Annual Review*, pp. 1026–1033. July 22–27, 2007, Golden, Colorado. American Institute of Physics, Melville, New York.

Connolly GD, MJS Lowe, SI Rokhlin and JAG Temple. 2008b. "Use of Fermat's Principle to Aid the Interpretation of the Ultrasonic Inspection of Anisotropic Welds." In *Review of Progress in Quantitative Nondestructive Evaluation, 34th Annual Review*, pp. 1018–1025. July 22–27, 2007, Golden, Colorado. American Institute of Physics, Melville, New York.

Connolly GD, MJS Lowe, SI Rokhlin and JAG Temple. 2009. "Imaging of Simple Defects in Austenitic Steel Welds Using a Simulated Ultrasonic Array." In *Proceedings of the 35th Annual Review of Progress in Quantitative Nondestructive Evaluation*, pp. 880–887. July 20–25, 2008, Chicago, Illinois. American Institute of Physics, Melville, New York.

Cumberland J. 1963. "Centrifugal Casting Techniques." *The British Foundryman* January:26–47.

Diaz AA, SR Doctor, BP Hildebrand, FA Simonen, GJ Schuster, ES Anderson, GP Mc Donald and RD Hasse. 1998. *Evaluation of Ultrasonic Inspection Techniques for Coarse-Grained Materials*. NUREG/CR-6594, PNNL-11171, U.S. Nuclear Regulatory Commission, Washington, D.C.

Doudet L, O Dupond, B Chassignole and E Abittan. 2008. "Ultrasonic Testing of Centrifugally Cast Stainless Steels: Influence of the Structure and the Characteristics of Beams." In *Proceedings of the 5th International Conference on NDE in Relation to Structural Integrity for Nuclear and Pressurized Components*. May 10–12, 2006, San Diego. Electric Power Research Institute, Palo Alto, California.

Ensminger D and LJ Bond. 2010. "Medical Applications of Ultrasonic Energy." In *Ultrasonics: Fundamentals, Technology and Applications, Third Edition*, 3rd (Revised and Expanded) ed. CRC Press.

EPRI. 2005. *Assessment of Cast Stainless Steel Inspection*. Report No. 1011600, Electric Power Research Company, Palo Alto, California.

Feuilly N, O Dupond, B Chassignole, J Moysan and G Corneloup. 2009. "Relation Between Ultrasonic Backscattering and Microstructure for Polycrystalline Materials." In *Proceedings of the 35th Annual Review of Progress in Quantitative Nondestructive Evaluation, Volume 28*, pp. 1216–1223. July 20–25, 2008, Chicago, Illinois. American Institute of Physics, Melville, New York.

Ghoshal G and JA Turner. 2009. "Diffuse Ultrasonic Backscatter in a Two-Dimensional Domain." *Acta Mech* 205:35–49.

Goebbels K. 1980. "Structure Analysis by Scattered Ultrasonic Radiation." In *Research Techniques in Nondestructive Testing*, ed: RS Sharpe. Ch. 4. Academic Press, Inc., London. Vol. IV.

Goebbels K. 1986. "Ultrasonics for Microcrystalline Structure Examination." *Philosophical Transactions of the Royal Society of London* Series A, Mathematical and Physical Sciences (320):161–169.

Goebbels K. 1994. *Materials Characterization for Process Control and Product Conformity*. CRC Press, Boca Raton, Florida.

Good MS, BP Hildebrand and CM Batson. 1991. "Phase Mapping of Ultrasonic Fields Passed Through Centrifugally Cast Stainless Steel." In *Review of Progress in Quantitative Nondestructive Evaluation (QNDE), Vol. 10B*, pp. 1975–1982. July 15–20, 1990, La Jolla, California. Plenum Press, New York.

Harker AH, JA Ogilvy and JAG Temple. 1990. "Modeling Ultrasonic Inspection of Austenitic Welds." *Journal of Nondestructive Evaluation* 9(2):155–165.

Heasler PG and SR Doctor. 1996. *Piping Inspection Round Robin*. NUREG/CR-5068, PNL-10475, U.S. Nuclear Regulatory Commission, Washington, D.C.

Hudgell RJ and BS Gray. 1985. *The Ultrasonic Inspection of Austenitic Materials - State of the Art Report*. ND-R-1201(R), CSNI Report No. 94, UKAEA, Risley Nuclear Power Development Establishment, Risley, Warrington, United Kingdom.

Jenson F, T Fortuna and L Doudet. 2009. "Modeling of Ultrasonic Propagation in a Coarse Grain Structure." In *Proceedings of the 35th Annual Review of Progress in Quantitative Nondestructive Evaluation*, pp. 1201–1208. July 20–25, 2008, Chicago, Illinois. American Institute of Physics, Melville, New York.

Jeong YHP. 1987. *An Ultrasonic Material State Classifier For Elastically Anisotropic Materials*. Ph. D. Thesis, Drexel University, Philadelphia, Pennsylvania.

Jeong YHP and F Ammirato. 1989. "Ultrasonic Material Characterization of Cast Stainless Steel." In *ASME Pressure Vessels and Piping Conference, NDE-Vol. 5*, pp. 199–203. July 23–27, 1989, Honolulu, Hawaii. American Society of Mechanical Engineers, New York.

Kono N and A Baba. 2008. "Development of Phased Array Probes for Austenitic Weld Inspections Using Multi-Gaussian Beam Modeling, Volume 27." In *Review of Progress in Quantitative Nondestructive Evaluation, 34th Annual Review*, pp. 747–753. July 22–27, 2007, Golden, Colorado. American Institute of Physics, Melville, New York.

Kupperman DS, KJ Reimann and J Abrego-Lopez. 1987. "Ultrasonic NDE of Cast Stainless Steel." *NDT International* 20(3):145–152.

Kupperman DS, KJ Reimann and DI Kim. 1981. "Ultrasonic Characterization and Microstructure of Stainless Steel Weld Metal." In *Nondestructive Evaluation: Microstructural Characterization and Reliability Strategies*, pp. 199–216. October 5–9, 1980, Pittsburgh, Pennsylvania. The Metallurgical Society of AIME, Warrendale, Pennsylvania.

Lyons RG. 2004. *Understanding Digital Signal Processing, 2nd Edition*. Prentice-Hall, Upper Saddle River, New Jersey.

Malcolm AE, JA Scales and BA van Tiggelen. 2004. "Extracting the Green Function from Diffuse, Equipartitioned Waves." *Physical Review E* 70:4.

Miralles R and L Vergara. 1999. "Ultrasonic Characterization of Scattering Media by Higher Order Spectra: A Cumulant Derivation." In *IEEE Signal Processing Workshop on High-Order Statistics (SPW-HOS'99)*, pp. 367–370. June 14–16, 1999, Madison, Wisconsin.

Miralles R, L Vergara and J Gosalbez. 2004. "Material Grain Noise Analysis by Using Higher-Order Statistics." *Signal Processing, IEEE Transactions on* 84(1):197–205.

Moysan J and G Corneloup. 2000. "Ultrasounds Back-Scattering Measurements for New Anisotropy Indicator Construction." In *15th World Conference on Nondestructive Testing*. October 15–21, 2000, Rome.

Nageswaran CRB and A Whittle. 2008. "Immersion Transmit-Receive Longitudinal Phased Array Probe for Stainless Steel." *Insight* 50(12):673–678.

Northcott L and V Dickin. 1944. "The Influence of Centrifugal Casting (Horizontal Axis) Upon the Structure and Properties of Metals." *The Journal of the Institute of Metals* LXX:301–323.

Northcott L and D McLean. 1945. "The Influence of Centrifugal Casting Upon the Structure and Properties of Steel." *The Journal of the Iron and Steel Institute* CLI:303–328.

Ogilvy JA. 1988. "Ultrasonic Propagation in Anisotropic Welds and Cast Materials." In *Mathematical Modelling in Non-Destructive Testing*. September 1986, Jesus College, Cambridge. Clarendon Press, Oxford (1988). Based on the proceedings of a conference organized by the Institute of Mathematics.

Pao Y-H. 1983. "Elastic Waves in Solids." *Transactions of the ASME* 50:1152–1164.

Papadakis EP. 1965. "Influence of Preferred Orientation on Ultrasonic Grain Scattering." *Journal of Applied Physics* 36(5):1738–1740.

Punurai W, J Jarzynski, J Qu, KE Kurtis and LJ Jacobs. 2007. "Characterization of Dissipation Losses in Cement Paste with Diffuse Ultrasound." *Mechanics Research Communications* 37:289–294.

Ramamoorthy SK, Y Kane and JA Turner. 2004. "Ultrasound Diffusion for Crack Depth Determination in Concrete." *Journal of Acoustical Society of America* 115(2).

Ramuhalli P, MS Good, AA Diaz, MT Anderson, BE Watson, TJ Peters, M Dixit and LJ Bond. 2009. *Ultrasonic Characterization of Cast Austenitic Stainless Steel Microstructure: Discrimination between Equiaxed- and Columnar-Grain Material – An Interim Study*. PNNL-18912, Pacific Northwest National Laboratory, Richland, Washington.

Ruud CO, AA Diaz and MT Anderson. 2009. *Literature Review - Grain Structure Identification and Fabrication Parameters of Cast Austenitic Stainless Steel (CASS) Piping*. PNNL-19002, Pacific Northwest National Laboratory, Richland, Washington.

Scales JA and AE Malcolm. 2003. "Laser Characterization of Ultrasonic Wave Propagation in Random Media." *Physical Review E* 67:7.

Segura A, P Lanceleur, J-F De Belleval, J-M Gherbezza and F Lesage. 2009. "Influence of Anisotropy for the Characterization of Internal Imperfections in Pipes by Ultrasonic Non-Destructive Testing." *NDT.net* 2009-05.

Sgard FC, N Atalla and J Nicolas. 2000. "A Numerical Model for the low Frequency Diffuse Field Sound Transmission Loss of Double-Wall Sound Barriers with Elastic Porous Linings." *Journal of Acoustical Society of America* 108(6):2865–2872.

Silverstein SD and LJ Thomas. 1993. "Analytical Comparison of Sensor Signal Processing Enhancements for NDT Synthetic Aperture Ultrasonic Imaging." *IEEE Transactions on Image Processing* 2(1):60–67.

Steele JH and JL McCall. 1984. *STP839, Practical Applications of Quantitative Metallography*. ASTM International, West Conshohocken, Pennsylvania.

Temple JAG and JA Ogilvy. 1992. *Propagation of Ultrasonic Elastic Waves in Centrifugally Cast Austenitic Steel*. AEA-RS-4223, AEA Reactor Services (Div. AEA Technology).

Thompson RB, FJ Margetan, P Haldipur, L Yu, A Li, P Panetta and H Wasan. 2008. "Scattering of Elastic Waves in Simple and Complex Polycrystals." *Wave Motion* 45(5):655–674.

Turner JA. 1999. "Elastic Wave Propagation and Scattering in Heterogeneous, Anisotropic Media: Textured Polycrystalline Materials." *The Journal of the Acoustical Society of America* 106(2):541–552.

Turner JA and RL Weaver. 1995. "Time Dependence of Multiply Scattered Diffuse Ultrasound in Polycrystalline Media." *The Journal of the Acoustical Society of America* 97(5):2639–2644.

Weaver RL. 1982. "On Diffuse Fields in Solid Media." *Journal of Acoustical Society of America* 71(6):1608–1609.

Weaver RL. 1998. "Ultrasonics in an Aluminum Foam." *Ultrasonics* 36:435–442.

Weaver RL and OI Lobkis. 2000. "Temperature Dependence of Diffuse Field Phase." *Ultrasonics* 38:491–494.

Weaver RL and OI Lobkis. 2001. "On the Emergence of the Green's Function in the Correlations of a Diffuse Field." *Journal of Acoustical Society of America* 110(6):3011–3017.

Weaver RL and OI Lobkis. 2004. *Fluctuations in Diffuse Field-Field Correlations and the Emergence of the Green's Function in Open Systems*. University of Illinois at Urbana–Champaign, Urbana, Illinois.

Weaver RL and OI Lobkis. 2005. *The Mean and Variance of Diffuse Field Correlations in Finite Bodies*. University of Illinois at Urbana–Champaign, Urbana, Illinois.

Weaver RL and W Sachse. 1994. "Diffusion of Ultrasound in a Glass Bead Slurry." *Journal of Acoustical Society of America* 97(4):2094-2102.

Willems H and K Goebbels. 1982. "Characterization of Microstructure by Scattered Ultrasonic Waves." In *Tenth World Conference on Non-Destructive Testing*, pp. 39–45. August 24–26, 1982, Moscow, Russia.

Pacific Northwest
NATIONAL LABORATORY

U.S. DEPARTMENT OF
ENERGY

Proudly Operated by Battelle *Since 1965*

902 Battelle Boulevard
P.O. Box 999
Richland, WA 99352
1-888-375-PNNL (7665)
www.pnl.gov